Forward tracking of complex trajectories with non-Standard N-Trailers of non-minimum-phase kinematics avoiding a jackknife effect

Maciej Marcin Michałek & Dariusz Pazderski

Published online: 21 Mar 2018.

Submit your article to this journal

Article views: 902

View related articles

View Crossmark data

Citing articles: 6 View citing articles

Taylor & Francis
Taylor & Francis Group

Forward tracking of complex trajectories with non-Standard N-Trailers of non-minimum-phase kinematics avoiding a jackknife effect

Maciej Marcin Michałek ⬤ and Dariusz Pazderski ⬤

Institute of Automation and Robotics, Faculty of Computing, Poznań University of Technology (PUT), Poznań, Poland

ABSTRACT

It is a common conviction that forward motion control of tractor-trailer vehicles is a substantially simpler problem relative to reversing with trailers. This opinion may be misleading when considering the N-trailer vehicles moving forward with positive hitching offsets when a guidance point is located on a trailer. Due to the non-minimum-phase nature of vehicle kinematics, closing a feedback from a trailer posture can lead to the jackknife effect in this case. So far, there has been no solution to this problem for the N-trailers admitting trajectories of a varying curvature. To fill this gap, we propose a scalable and modular control strategy applicable to the N-trailer vehicles equipped solely with off-axle interconnections. The concept relies on a transformation of the control problem posed for the non-minimum-phase kinematics into a corresponding problem formulated for a virtual vehicle of minimum-phase kinematics, which can be solved by using the recently proposed cascade-like controller.

1. Introduction

The need of accurate guiding the (last) trailer of tractor-trailer vehicles moving forward appears in various practical applications. For instance, positioning of the urban articulated buses is often prohibited by law in a backward manner when manoeuvering on urban streets and in vicinity of bus stations (Tan & Huang, 2014). Agricultural tasks with tractor-trailers are performed mostly in the forward motion strategy (Auat Cheein et al., 2016; Backman, Oksanen, & Visala, 2012; Karkee & Steward, 2010; Werner, Kormann, & Mueller, 2013). Finally, some loading/unloading tasks require positioning of the trailer(s) when a vehicle is moving forward. Therefore, considering the forward tracking problem for the articulated vehicles seems justified by the practical needs.

Numerous solutions to the trajectory tracking task for the tractor-trailer vehicles have been proposed in the literature so far. However, most of them have been devoted to the backward-motion case, either for tractor-trailers kinematics with some particular number of trailers (usually for 1-trailers only) (Bullo & Murray, 1996; Kayacan, Ramon, & Saeys, 2016; Khalaji & Moosavian, 2014; Kim & Oh, 2002; Lamiraux, Sekhavat, & Laumond, 1999; Pradalier & Usher, 2008; Yuan & Zhu, 2016; Yue, Hou, Gao, & Chen, 2018) or for vehicles equipped solely with on-axle hitches (the kinematics of which belong to differentially flat systems) (Cheng, Wang, Zhang, & Wang, 2017; Khalaji & Moosavian, 2016; Morin & Samson, 2008b; Pazderski, Waśkowicz, & Kozłowski, 2015). Design of a trajectory-tracking control strategy for *truly* N-trailer robotic vehicles (i.e. those admitting an *arbitrary* number of trailers) equipped with

non-zero hitching offsets, and where the guidance point of a vehicle is located on a (last) trailer, is generally a more difficult problem (Chung, Park, Yoo, Roh, & Choi, 2011; Michałek, 2017). It is a consequence of specific properties characterising kinematics of such systems which are no more differentially flat (Michałek, 2013; Rouchon, Fliess, Levine, & Martin, 1993). One of the most commonly mentioned and addressed properties refers to the joint-instability of a vehicle chain in backward motion conditions. Therefore, the forward motion tasks are usually treated as much simpler due to structural stability of the vehicle's joint-dynamics in these motion conditions. However, it does not reflect the full complexity of the problem. Namely, if the N-trailer contains positive hitching offsets and moves forward (i.e. with positive longitudinal velocities of the vehicle segments) one must expect the non-minimum-phase effects in dynamics between the angular configuration variables of a vehicle and the angular velocity of a tractor (a detailed treatment of this issue can be found in Michałek (2013); see also Martinez, Morales, Mandow, and Garcia-Cerezo (2008)). It is well known (see, e.g. Aguiar, Hespanha, & Kokotović, 2008; Hoagg & Bernstein, 2007; Seron, Braslavsky, & Goodwin, 1997 and references cited therein) that the non-minimum-phasiness of a plant imposes fundamental limitations on the feedback control design and may restrict performance attainable in a closed-loop system. As a consequence, in the case of automatically guided N-trailers, the non-minimum-phasiness may be the reason of the so-called jackknife effect, even in forward motion conditions, which is manifested by the undesirable (and usually destructive) folding of a vehicle in its passive joints (Chiu & Goswami, 2014). This

---

particular limitation has been observed and formally explained by the authors of Bolzern, DeSantis, and Locatelli (2001) and Michałek (2017) in the context of cascade-like control design. A simple *remedy* applied by most investigators in the case of forward motion conditions is to move the guidance point of a vehicle to the tractor segment which substantially simplifies the control design problem (Astolfi, Bolzern, & Locatelli, 2004; Bolzern et al., 2001; DeSantis, Bourgeot, Todeschi, & Hurteau, 2002; Ma, Niu, Xie, & Lin, 2014; Yuan & Huang, 2006). However, this simple trick also essentially changes an underlying control objective, which becomes unsuitable when a motion task is defined with respect to a trailer, rather than to a tractor segment. An alternative approach, (although not so simple) is to approximate the N-trailer kinematics by a differentially flat system, which for a vehicle containing the non-zero hitching offsets is possible only locally and only in special cases; see Lizarraga, Morin, and Samson (2001), and Bolzern, DeSantis, Locatelli, and Masciocchi (1998).

As a consequence of the above-mentioned difficulties, any generic solution to the forward tracking control problem for truly N-trailers with positive hitching offsets and the guidance point located on a trailer has not been presented so far, except some preliminary or restricted results. Namely, a solution to the path-following problem in forward motion conditions for the non-minimum-phase kinematics has been proposed in Cariou, Lenain, Thuilot, and Martinet (2010), and Leng and Minor (2017) for a tractor-single-trailer vehicle. Both solutions are interesting, however, only Leng and Minor (2017) presents a control strategy which deals with the varying-curvature paths. It is not clear if they can be (easily) generalised to the N-trailer case. To the authors' best knowledge, the only work addressing the N-trailers in the context of control design for forward motion conditions with a guidance point located on the last trailer is Bolzern et al. (1998), where the *ghost-vehicle* approach was proposed by applying a feedback-linearisation concept for the case of constant-curvature reference paths. However, scalability of this solution (with respect to a number of trailers) is essentially limited requiring derivation of a control law for any particular case of the N-trailer structure, where complexity of the controller substantially increases with a number of trailers.

In view of the above comments, we propose a cascade-like scalable control strategy for *truly* N-trailer robots of *non-minimum-phase kinematics* containing only non-zero hitching offsets to address the trajectory tracking task under *forward motion conditions* with a *guidance point located on a last trailer*. A general concept proposed here (motivated by Bolzern et al., 1998) relies on a transformation of an original control task stated for a real vehicle of non-minimum-phase kinematics into a corresponding control problem for a virtual tractor-trailers vehicle of minimum-phase kinematics, which shares a common tractor with the real N-trailer. Designing a feedback controller for a virtual vehicle and applying it to the real tractor helps in avoiding a jackknife phenomenon, and simultaneously enables to obtain an asymptotic tracking of even complex reference trajectories in forward motion conditions. To our best knowledge, it is the first solution to the forward tracking problem devised for truly N-trailers of non-minimum-phase kinematics which admits reference trajectories of a varying curvature. In contrast to Bolzern et al. (1998), we do not apply any linearisation

Figure 1. REAL nSNT vehicle (black) and its VIRTUAL nSNT minimum-phase counterpart (gray) in a global frame {*G*}.

concept, and provide a modular non-singular controller applicable to N-trailer structures with all positive or mixed (positive and negative) hitching offsets. The approach proposed in this paper builds upon Michałek (2017), however, it is (non-trivially) adopted to address the forward tracking problem for vehicles with non-minimum-phase kinematics, not considered in Michałek (2017).

2. Vehicle kinematics and problem formulation

2.1 Kinematic model of the real and virtual vehicles

Let us consider the N-trailer vehicle presented in Figure 1, which consists of an active unicycle-like tractor and an arbitrary number of *N* passive trailers interconnected with passive rotary joints. For our purposes, we will distinguish two vehicles: the REAL vehicle (denoted in black in Figure 1) representing a physically available N-trailer, and the VIRTUAL vehicle which is only an imaginary object. The vehicles share a common tractor and possess the same number of segments. The aim of introducing the virtual vehicle will be clarified in Section 3.1.

The configuration and control input of the real vehicle will be represented, respectively, by

$$\boldsymbol{q} \triangleq \begin{bmatrix} \boldsymbol{\beta} \\ \boldsymbol{q}_N \end{bmatrix} \in \mathbb{T}^N \times \mathbb{R}^3 \quad \text{and} \quad \boldsymbol{u}_0 = \begin{bmatrix} \omega_0 \\ v_0 \end{bmatrix} \in \mathbb{R}^2, \qquad (1)$$

where the joint-angles vector $\boldsymbol{\beta} = [\beta_1 \ \ldots \ \beta_N]^\top$ determines a vehicle *shape* described on the N-dimensional torus $\mathbb{T}^N = \mathbb{S}^1 \times \cdots \times \mathbb{S}^1$ (N times), vector $\boldsymbol{q}_N = [\theta_N \ x_N \ y_N]^\top$ denotes a posture of a last trailer (called the *guidance segment*), while ω_0 and v_0 are, respectively, an angular tractor velocity and a longitudinal velocity of a wheels-axle midpoint of the tractor. Segments of the real vehicle are characterised by two kinds of kinematic parameters: trailer lengths $L_i > 0$ and hitching offsets $L_{hi} \in \mathbb{R}$. The ith hitching offset is positive ($L_{hi} > 0$) if a hitching point in located *behind* a wheels-axle of the $(i - 1)$st vehicle's segment, it is negative if a hitching point is located *in front* of the wheels-axle, whereas

$L_{hi} = 0$ when the hitching point is located exactly on the wheels-axle (see Figure 1: on the picture $L_{hN} > 0$ but $\bar{L}_{hN} < 0$).

We assume what follows:

A1. $L_{hi} \neq 0 \ \forall \ i = 1, \ldots, N$ and $\exists \ i \ L_{hi} > 0$.

Assumption A1 restricts our considerations to the class of the so-called non-Standard N-Trailers (nSNT – see e.g. Michałek, 2017) in which the signs of hitching offsets can be mixed (we admit both positive and negative offsets in the same kinematic chain), while at least one of the offsets is positive. The latter makes the control problem especially difficult in the forward motion strategy. It is due to the fact (formally addressed in Michałek, 2013) that kinematics of the N-trailer moving with positive longitudinal velocity reveals the non-minimum-phase property in the dynamic route between the angular velocity of the tractor and angular configuration variables of the vehicle if hitching offsets are positive.

Assuming the rolling-without-slipping motion condition for all the vehicle's wheels, every ith vehicle segment ($i = 0, \ldots, N$) can be treated as a unicycle with kinematics defined as follows (we use notation $s\alpha = \sin \alpha$ and $c\alpha = \cos \alpha$ for conciseness):

$$\dot{q}_i = G(q_i)u_i = \begin{bmatrix} 1 & 0 & 0 \\ 0 & c\theta_i & s\theta_i \end{bmatrix}^\top u_i, \quad i = 0, \ldots, N, \qquad (2)$$

with posture $q_i = [\theta_i \ x_i \ y_i]^\top \in \mathbb{R}^3$ and input velocity $u_i = [\omega_i \ v_i]^\top \in \mathbb{R}^2$. According to Michałek (2013) and Michałek (2017), one can express the N-trailer kinematics in the form of a driftless system

$$\underbrace{\begin{bmatrix} \dot{\boldsymbol{\beta}} \\ \dot{q}_N \end{bmatrix}}_{\dot{q}} = \underbrace{\begin{bmatrix} S_\beta(\boldsymbol{\beta}) \\ ----- \\ S_N(\boldsymbol{\beta}, q_N) \end{bmatrix}}_{S(q)} u_0 = \begin{bmatrix} c^\top \Gamma_1(\beta_1) \\ c^\top \Gamma_2(\beta_2)J_1(\beta_1) \\ \vdots \\ c^\top \Gamma_N(\beta_N)J_{N-1}^1(\boldsymbol{\beta}) \\ ----------- \\ c^\top J_N^1(\boldsymbol{\beta}) \\ d^\top J_N^1(\boldsymbol{\beta})c\theta_N \\ d^\top J_N^1(\boldsymbol{\beta})s\theta_N \end{bmatrix} u_0,$$

$$(3)$$

where $\Gamma_i(\beta_i) \triangleq I_{2\times2} - J_i(\beta_i), I_{2\times2} \in \mathbb{R}^{2\times2}$ is an identity matrix, $J_i^1(\boldsymbol{\beta}) \triangleq J_i(\beta_i) \ldots J_1(\beta_1), c^\top \triangleq [1 \ 0], d^\top \triangleq [0 \ 1]$, while

$$J_i(\beta_i) = \begin{bmatrix} -(L_{hi}/L_i)c\beta_i & (1/L_i)s\beta_i \\ L_{hi} \ s\beta_i & c\beta_i \end{bmatrix} \qquad (4)$$

is a velocity transformation matrix, which has got a well-defined inverse $J_i^{-1}(\beta_i)$ under Assumption A1. Matrix (4) transforms velocities u_i and u_{i-1} of any two neighbouring vehicle segments according to the formula: $u_i = J_i(\beta_i)u_{i-1}$. By iterative application of this transformation, and its inverse, one gets two key mappings between velocities along a vehicle chain (valid for $i \in \{1, \ldots, N\}$)

$$u_i = \prod_{j=i}^{1} J_j(\beta_j)u_0, \qquad u_{i-1} = \prod_{j=i}^{N} J_j^{-1}(\beta_j)u_N, \qquad (5)$$

which will be essential for further considerations. It is worth to stress once again that kinematics (3) under Assumption A1 reveals the non-minimum-phase property in the forward motion conditions (for more details, we refer a reader to Michałek, 2013). This structural property is a main source of difficulties for a control strategy design discussed in Section 3.

The virtual vehicle can be described, by analogy to the real vehicle, with virtual configuration and input vectors

$$\bar{q} \triangleq \begin{bmatrix} \bar{\boldsymbol{\beta}} \\ \bar{q}_N \end{bmatrix} \in \mathbb{T}^N \times \mathbb{R}^3, \qquad \bar{u}_0 \equiv u_0 \in \mathbb{R}^2 \qquad (6)$$

denoted with a bar mark above particular symbols. The equivalence $\bar{u}_0 \equiv u_0$ results from the assumption that the tractor is a common segment for both vehicles. For the virtual vehicle, we assume what follows:

A2. $\bar{L}_{hi} = -h_i |L_{hi}| \ \forall \ i = 1, \ldots, N, \quad h_i > 0,$
A3. $\bar{L}_i > |\bar{L}_{hi}| \ \forall \ i = 1, \ldots, N.$

Assumption A2 imposes solely negative hitching offsets in the virtual vehicle chain, which makes its kinematics minimum-phase in the forward motion conditions (see Michałek, 2013) – it is the key difference between kinematics of the virtual vehicle and the real one. Moreover, by introducing the design factors h_i we admit different lengths of hitching offsets for the virtual vehicle than the lengths of the offsets present in the real vehicle. It will be shown in Section 5.1 that factors h_i are useful in adjusting a measurement-noise sensitivity of a closed-loop system. A3 comes from obvious mechanical constraints, however, we do not impose any other special limitation on selection of $\bar{L}_i$. It will be shown in Section 5.1 that the values of parameters $\bar{L}_i$ influence a transient performance of a closed-loop system and may be treated as design parameters.

Introducing the velocity transformation matrix for the virtual vehicle as

$$\bar{J}_i(\bar{\beta}_i) = \begin{bmatrix} -(\bar{L}_{hi}/\bar{L}_i) \, c\bar{\beta}_i & (1/\bar{L}_i) \, s\bar{\beta}_i \\ \bar{L}_{hi}s\bar{\beta}_i & c\bar{\beta}_i \end{bmatrix}, \qquad (7)$$

one can write kinematic relations and velocity mappings for the virtual vehicle in the same forms as in Equation (2), (3) and (5), respectively, but using the symbols denoted with a bar mark.

2.2 Underlying mappings of direct and inverse kinematics

Let us define the direct and inverse kinematic mappings for the nSNT structures which will be instrumental for the subsequent considerations.

The *inverse posture kinematics* $\text{inv}Q^i : \mathbb{R}^3 \times \mathbb{T}^N \to \mathbb{R}^3$ is used to compute a posture $q_i = \text{inv}Q^i(q_N, \boldsymbol{\beta})$ of the ith vehicle segment (cf. Equation (2)) upon the knowledge of the guidance segment posture $q_N = [\theta_N \ x_N \ y_N]^\top$ and the joint angles $\boldsymbol{\beta}$ of a vehicle. Based on geometrical arguments inferred from Figure 1, one can write the following iterative relationships: $\theta_i = \theta_{i+1} + \beta_{i+1}, x_i = x_{i+1} + L_{i+1}c\theta_{i+1} + L_{hi+1}c\theta_i$, and $y_i = y_{i+1} + L_{i+1}s\theta_{i+1} + L_{hi+1}s\theta_i$, which are valid for $i \in \{0, \ldots, N-1\}$.

Next, the iterative equations can be reformulated into a non-iterative form

$$\text{inv}\boldsymbol{Q}^i(\boldsymbol{q}_N, \boldsymbol{\beta}) \triangleq \begin{bmatrix} \theta_N + \sum_{l=N}^{i+1} \beta_l \\ x_N + \sum_{j=N}^{i+1}(L_j c\theta_j + L_{hj}c\theta_{j-1}) \\ y_N + \sum_{j=N}^{i+1}(L_j s\theta_j + L_{hj}s\theta_{j-1}) \end{bmatrix}, \qquad (8)$$

where $i \in \{0, \ldots, N-1\}$, while $\theta_j = \theta_N + \sum_{l=N}^{j+1} \beta_l$ and $\theta_{j-1} = \theta_N + \sum_{l=N}^{j} \beta_l$ are computable solely upon $\boldsymbol{q}_N$ and $\boldsymbol{\beta}$ according to the first row of Equation (8).

The *direct posture kinematics* $\boldsymbol{Q}^i : \mathbb{R}^3 \times \mathbb{T}^N \to \mathbb{R}^3$ is used to compute a posture $\boldsymbol{q}_i = \boldsymbol{Q}^i(\boldsymbol{q}_0, \boldsymbol{\beta})$ of the ith vehicle segment upon the knowledge of the tractor posture $\boldsymbol{q}_0 = [\theta_0 \ x_0 \ y_0]^\top$ and the joint angles $\boldsymbol{\beta}$ of a vehicle. Recalling the iterative relations formulated above Equation (8), one can write: $\theta_i = \theta_{i-1} - \beta_i$, $x_i = x_{i-1} - L_i c\theta_i - L_{hi}c\theta_{i-1}$, and $y_i = y_{i-1} - L_i s\theta_i - L_{hi}s\theta_{i-1}$, valid for $i \in \{1, \ldots, N\}$. One can reformulate these equations into a non-iterative form

$$\boldsymbol{Q}^i(\boldsymbol{q}_0, \boldsymbol{\beta}) \triangleq \begin{bmatrix} \theta_0 - \sum_{l=1}^{i} \beta_l \\ x_0 - \sum_{j=1}^{i}(L_j c\theta_j + L_{hj}c\theta_{j-1}) \\ y_0 - \sum_{j=1}^{i}(L_j s\theta_j + L_{hj}s\theta_{j-1}) \end{bmatrix}, \qquad (9)$$

where $i \in \{1, \ldots, N\}$, while $\theta_j = \theta_0 - \sum_{l=1}^{j} \beta_l$ and $\theta_{j-1} = \theta_0 - \sum_{l=1}^{j-1} \beta_l$ are computable solely upon $\boldsymbol{q}_0$ and $\boldsymbol{\beta}$ according to the first row of Equation (9).

By analogy to the direct and inverse kinematics for postures, let us define their counterparts in the domain of velocities. Recalling relationships (5), one can introduce two mappings $\boldsymbol{V}^i, \text{inv}\boldsymbol{V}^i : \mathbb{R}^2 \times \mathbb{T}^N \to \mathbb{R}^2$ called the *direct velocity kinematics* and *inverse velocity kinematics*, respectively, of the forms

$$\boldsymbol{V}^i(\boldsymbol{u}_0, \boldsymbol{\beta}) \triangleq \prod_{j=i}^{1} \boldsymbol{J}_j(\beta_j)\boldsymbol{u}_0, \qquad (10)$$

$$\text{inv}\boldsymbol{V}^i(\boldsymbol{u}_N, \boldsymbol{\beta}) \triangleq \prod_{j=i+1}^{N} \boldsymbol{J}_j^{-1}(\beta_j)\boldsymbol{u}_N. \qquad (11)$$

The direct velocity kinematics allows computing velocities $\boldsymbol{u}_i = \boldsymbol{V}^i(\boldsymbol{u}_0, \boldsymbol{\beta})$ of the ith vehicle segment (cf. Equation (2)) based on the tractor velocities $\boldsymbol{u}_0$ and the joint angles $\boldsymbol{\beta}$ of a vehicle. On the other hand, the inverse velocity kinematics return velocity vector $\boldsymbol{u}_i = \text{inv}\boldsymbol{V}^i(\boldsymbol{u}_N, \boldsymbol{\beta})$ computed upon velocities $\boldsymbol{u}_N$ of the last trailer and the joint angles $\boldsymbol{\beta}$ of a vehicle.

Remark 2.1: From now on, by writing $\text{inv}\bar{\boldsymbol{Q}}^i$ and $\text{inv}\bar{\boldsymbol{V}}^i$ or $\bar{\boldsymbol{Q}}^i$ and $\bar{\boldsymbol{V}}^i$ (with the bar mark above) we will understand the inverse or direct kinematics, respectively, computed by using the appropriate parameters $\bar{L}_j$ and $\bar{L}_{hj}$ of the *virtual vehicle* instead of the

real vehicle's parameters L_j and L_{hj}. This distinguishing will be important in the following sections.

2.3 Reference trajectories and control problem formulation

For the real nSNT vehicle, we prescribe the reference guidance trajectory $\boldsymbol{q}_{Nr}(t) = [\theta_{Nr}(t) \ x_{Nr}(t) \ y_{Nr}(t)]^\top \in \mathbb{R}^3$ admissible for the unicycle kinematics, that is,

$$\boldsymbol{q}_{Nr}(t) : \ \forall t \geq 0 \quad \dot{\boldsymbol{q}}_{Nr}(t) = \boldsymbol{G}(\boldsymbol{q}_{Nr}(t))\boldsymbol{u}_{Nr}(t), \qquad (12)$$

where the form of $\boldsymbol{G}(\boldsymbol{q}_{Nr})$ results from Equation (2), while $\boldsymbol{u}_{Nr}(t) = [\omega_{Nr}(t) \ v_{Nr}(t)]^\top$ is a reference guidance velocity such that

(r1) $\forall t \geq 0 \ v_{Nr}(t) > 0$ (persistent forward reference motion),
(r2) $\sup_{t \geq 0} \| \boldsymbol{u}_{Nr}(t) \| \leq \delta_1$, $\sup_{t \geq 0} \| \dot{\boldsymbol{u}}_{Nr}(t) \| \leq \delta_2$, for some finite upper bounds $\delta_1, \delta_2 > 0$.

With the reference guidance trajectory $\boldsymbol{q}_{Nr}(t)$ we associate a reference shape trajectory $\boldsymbol{\beta}_r(t)$ compatible with $\boldsymbol{q}_{Nr}(t)$ by satisfying the reference shape kinematics (the exogenous system)

$$\dot{\boldsymbol{\beta}}_r \overset{(3)}{=} \boldsymbol{S}_\beta(\boldsymbol{\beta}_r)\boldsymbol{u}_{0r} \overset{(5)}{=} \boldsymbol{S}_\beta(\boldsymbol{\beta}_r) \prod_{j=1}^{N} \boldsymbol{J}_j^{-1}(\beta_{jr})\boldsymbol{u}_{Nr} \qquad (13)$$

expressed with the same reference velocity $\boldsymbol{u}_{Nr}$ used in Equation (12). There is a conjecture that there exist 2^N steady solutions $\boldsymbol{\beta}_r$ of Equation (13) compatible with the same guidance trajectory $\boldsymbol{q}_{Nr}(t)$ (that is, corresponding to the same velocity $\boldsymbol{u}_{Nr}(t)$). Most of them, however, lead to the jackknife effect and usually should be avoided in practical applications. Therefore, amongst all the possible reference trajectories $\boldsymbol{q}_r(t) = [\boldsymbol{\beta}_r^\top(t) \ \boldsymbol{q}_{Nr}^\top(t)]^\top$ satisfying Equation (12) and (13) we will consider only the so-called S-P (Segment-Platooning) trajectories (Michałek, 2017), which guarantee the same signs for reference longitudinal velocities of all the vehicle segments, i.e.

$$\boldsymbol{q}_r(t) : \ v_{ir}(t)v_{i-1r}(t) > 0 \quad \forall t \geq 0, \ i = 1, \ldots, N \qquad (14)$$

where $v_{i-1r} \overset{(5)}{=} [0 \ 1] \cdot \prod_{j=i}^{N} \boldsymbol{J}_j^{-1}(\beta_{jr})\boldsymbol{u}_{Nr}$. The S-P property (14) is highly desirable because it prevents the jackknife effect along a reference trajectory $\boldsymbol{q}_r(t)$.

Introducing now the shape tracking error and the guidance tracking error, respectively, as

$$\tilde{\boldsymbol{\beta}} \triangleq \boldsymbol{\beta}_r - \boldsymbol{\beta}, \qquad \boldsymbol{e}_N \triangleq \boldsymbol{q}_{Nr} - \boldsymbol{q}_N = \begin{bmatrix} e_\theta \ e_x \ e_y \end{bmatrix}^\top, \qquad (15)$$

one can formulate the following control problem.

Problem 2.1: Find a feedback control strategy for input $\boldsymbol{u}_0$ of kinematics (3) under Assumption A1, which ensures boundedness and asymptotic convergence of tracking errors (15) to zero for reference trajectories $\boldsymbol{q}_r(t)$ satisfying S-P condition (14) and requirements (r1)–(r2).

3. Tracking control law

3.1 Control strategy description: the virtual-vehicle concept

At the first attempt, one could try to apply the cascade-like control law proposed in Michałek (2017) to solve the Problem 2.1 stated above. Unfortunately, the analysis provided in Michałek (2017) reveals that application of this control law to the N-trailer kinematics satisfying Assumption A1 will inevitably lead to the undesirable jackknife effect (see the results in Section 5.1). This is a direct consequence of the non-minimum-phase kinematics of the real N-trailer vehicle in the forward motion conditions (Michałek, 2013).

In order to prevent the jackknife phenomenon, we propose to apply the virtual-vehicle concept (motivated by Bolzern et al., 1998) using the virtual vehicle introduced in Section 2 which, in contrast to the real vehicle, possesses the minimum-phase kinematics in the forward motion conditions under Assumption A2. A general idea is to transform the *ill-conditioned* control problem posed for the real vehicle (see Problem 2.1) into a corresponding problem being well-conditioned for the virtual vehicle. Next, we propose to apply the cascade-like control law presented in Michałek (2017) to the virtual vehicle which should guarantee asymptotic guidance of its last trailer along a corresponding reference trajectory without a jackknife effect. The question is: how to ensure that asymptotic stability obtained for a closed-loop system with the virtual vehicle entails solution to Problem 2.1 for the real vehicle? One can achieve it in the control system illustrated in Figure 2 by using two key transformations between the real and virtual kinematics (denoted as $\mathbf{\Gamma}$ and $\mathbf{H}$ in Figure 2), and recalling that the tractor links the two vehicles together. Let us explain the roles played by the two mappings.

Mapping $\mathbf{\Gamma}$ transforms the prescribed reference guidance trajectory $\boldsymbol{q}_{Nr}(t)$ and the reference guidance velocity $\boldsymbol{u}_{Nr}(t)$ to the corresponding compatible reference signals, $\bar{\boldsymbol{q}}_{Nr}(t)$ and $\bar{\boldsymbol{u}}_{Nr}(t)$, for the virtual vehicle, i.e.

$$\begin{bmatrix} \bar{\boldsymbol{q}}_{Nr} \\ \bar{\boldsymbol{u}}_{Nr} \end{bmatrix} = \mathbf{\Gamma}(\boldsymbol{q}_{Nr}, \boldsymbol{u}_{Nr}) = \begin{bmatrix} \mathbf{\Gamma}_q(\boldsymbol{q}_{Nr}, \boldsymbol{u}_{Nr}) \\ \mathbf{\Gamma}_u(\boldsymbol{u}_{Nr}) \end{bmatrix}, \quad (16)$$

where the exact construction of mapping $\mathbf{\Gamma}$ will be explained in Section 3.2. With reference signals $\bar{\boldsymbol{q}}_{Nr}$ and $\bar{\boldsymbol{u}}_{Nr}$ we have to associate (by analogy to the real vehicle) the reference virtual shape configuration $\bar{\boldsymbol{\beta}}_r = [\bar{\beta}_{1r} \ \ldots \ \bar{\beta}_{Nr}]^\top$, which will be computed within mapping $\mathbf{\Gamma}$ as an auxiliary signal (see Section 3.2 and Figure 3) but will not be directly used in a control process.
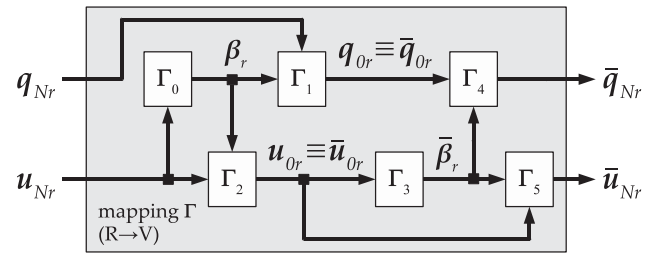
Figure 3. Functional scheme explaining computational stages required for mapping $\mathbf{\Gamma}$ used in the reference trajectory generator for the nSNT vehicle.

A role of transformation $\mathbf{H}$ is to establish a correspondence between the guidance segment posture $\bar{\boldsymbol{q}}_N$ of the virtual vehicle and measurable configuration $\boldsymbol{q}$ of the real vehicle. Such a correspondence can be obtained by the following transformation:

$$\bar{\boldsymbol{q}}_N = \boldsymbol{H}(\boldsymbol{q}_N, \boldsymbol{\beta}, \bar{\boldsymbol{\beta}}), \quad (17)$$

where the exact construction of mapping $\boldsymbol{H}$ will be explained in Section 3.2.

Having the two mappings, $\mathbf{\Gamma}$ and $\boldsymbol{H}$, let us introduce the virtual tracking errors (cf. Equation (15))

$$\bar{\tilde{\boldsymbol{\beta}}} \triangleq \bar{\boldsymbol{\beta}}_r - \bar{\boldsymbol{\beta}}, \qquad \bar{\boldsymbol{e}}_N \triangleq \bar{\boldsymbol{q}}_{Nr} - \bar{\boldsymbol{q}}_N = \begin{bmatrix} \bar{e}_\theta \ \bar{e}_x \ \bar{e}_y \end{bmatrix}^\top. \quad (18)$$

Since the virtual vehicle of minimum-phase kinematics meets all the requirements imposed in Michałek (2017) for the cascade-like controller to guarantee asymptotic stability of point $(\bar{\boldsymbol{e}}_N, \bar{\tilde{\boldsymbol{\beta}}}) = (\mathbf{0}, \mathbf{0})$ in forward motion conditions for the S-P trajectories, we propose the following feedback control law:

$$\boldsymbol{u}_0(t) \triangleq \prod_{j=1}^{N} \bar{\boldsymbol{J}}_j^{-1}(\bar{\beta}_j(t)) \, \boldsymbol{\phi}(\bar{\boldsymbol{e}}_N(t), t) \quad (19)$$

where $\boldsymbol{\phi}(\bar{\boldsymbol{e}}_N(t), t)$ is an outer-loop tracking control function devised for the unicycle kinematics and possessing some particular properties (see Remark 3.2). We suppose (it will be formally shown in Section 4) that by application of Equation (19) into a tractor – the common segment of both the virtual and the real vehicle – will lead to asymptotic tracking of the corresponding S-P trajectory $\bar{\boldsymbol{q}}_r(t) = [\bar{\boldsymbol{\beta}}_r^\top(t) \ \bar{\boldsymbol{q}}_{Nr}^\top(t)]^\top$ by the virtual vehicle and, as a consequence, will lead to asymptotic tracking the originally prescribed S-P trajectory $\boldsymbol{q}_r(t)$ by the real vehicle.
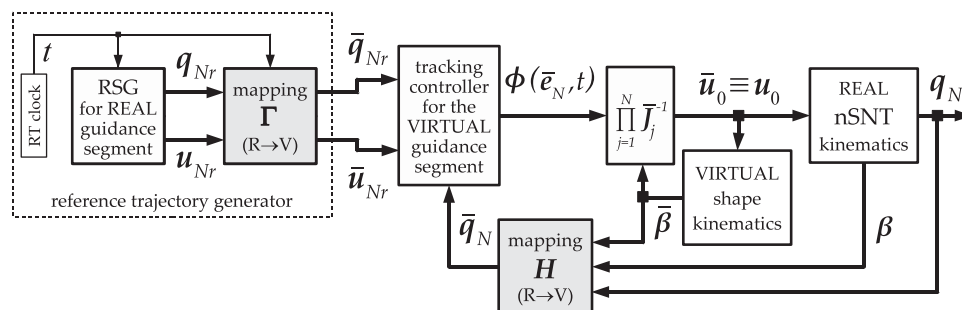
Figure 2. Block scheme of the proposed control system (RSG = reference signals generator, R→V denotes mapping from REAL to VIRTUAL vehicle).

The above reasoning expresses an underlying idea of the virtual vehicle approach.

Remark 3.1: The form of control law (19), together with Assumption A2, explains a necessity of introducing Assumption A1. Namely, if any ith hitching offset is of a zero length, the matrix $\bar{J}_i$ becomes singular and cannot be used in Equation (19).

Remark 3.2: It is worth noting that control law (19) has a modular structure since the outer-loop control function $\boldsymbol{\phi}(\bar{e}_N(t), t)$ represents any continuous and bounded asymptotic tracking control function developed for unicycle kinematics satisfying the following general properties (Michałek, 2017) (numerous control functions of this type can be found in the literature – see e.g. Canudas de Wit, Siciliano, & Bastin, 1996; Morin & Samson, 2008a):

(p1) $\boldsymbol{\phi}(\mathbf{0}, t) \equiv \bar{u}_{Nr}(t)$,
(p2) $\bar{u}_N(t) \equiv \boldsymbol{\phi}(\bar{e}_N(t), t)$ makes the point $\bar{e}_N = \mathbf{0}$ uniformly asymptotically stable in some domain $\mathcal{D}_E \subseteq \mathbb{R}^3$,
(p3) property (p2) entails $\| \boldsymbol{\phi}(\bar{e}_N(t), t) \| < \infty$ for all $t \geq 0$ and $\forall \bar{e}_N \in \mathcal{D}_E$.

Remark 3.3: The form of matrix $\bar{J}_j^{-1}(\bar{\beta}_j)$ in Equation (19) results from the inverse of the matrix from Equation (7), and it has to be evaluated upon the current shape configuration $\bar{\boldsymbol{\beta}}$ of the virtual vehicle. Therefore, angles $\bar{\beta}_j(t)$ need to be computed on-line by integration of the virtual shape kinematics $\dot{\bar{\boldsymbol{\beta}}} = \bar{S}_\beta(\bar{\boldsymbol{\beta}})\bar{u}_0$ (cf. Equation (3)), i.e.

$$\bar{\boldsymbol{\beta}}(t) = \bar{\boldsymbol{\beta}}(0) + \int_0^t \bar{S}_\beta(\bar{\boldsymbol{\beta}}(\tau))u_0(\tau)d\tau \qquad (20)$$

for $\bar{\boldsymbol{\beta}}(0) := \boldsymbol{\beta}(0)$ and $u_0 \equiv \bar{u}_0$ taken from Equation (19), cf. Figure 2.

Taking into account Equations (16) and (17), the control law (19) can be rewritten as follows:

$$u_0 \triangleq \prod_{j=1}^N \bar{J}_j^{-1}(\bar{\beta}_j) \, \boldsymbol{\phi}([\Gamma_q(q_{Nr}, u_{Nr}) - H(q_N, \boldsymbol{\beta}, \bar{\boldsymbol{\beta}})], t)$$

which explains the proposed control structure in a more comprehensive way (see Figure 2).

3.2 Description of mappings H and Γ

The objective of mapping $H : \mathbb{R}^3 \times \mathbb{T}^N \times \mathbb{T}^N \to \mathbb{R}^3$ is to compute the posture $\bar{q}_N = H(q_N, \boldsymbol{\beta}, \bar{\boldsymbol{\beta}})$ of the last virtual trailer applying a feedback dependent on a configuration of the real vehicle and using the virtual joint angles $\bar{\boldsymbol{\beta}}$ being a response (20) of the simulated virtual shape kinematics. Mapping H is defined as follows:

$$H(q_N, \boldsymbol{\beta}, \bar{\boldsymbol{\beta}}) \triangleq \bar{Q}^N \left(\text{inv}Q^0(q_N, \boldsymbol{\beta}), \bar{\boldsymbol{\beta}} \right), \qquad (21)$$

where $\text{inv}Q^0(q_N, \boldsymbol{\beta}) \overset{(8)}{=} q_0 \equiv \bar{q}_0$ returns a current posture of the tractor (a common segment for the real and virtual vehicles). The role of mapping H results from Figure 2 (cf. also Figure 1).

Mapping $\Gamma : \mathbb{R}^3 \times \mathbb{R}^2 \to \mathbb{R}^3 \times \mathbb{R}^2$ can be decomposed into six component mappings denoted by Γ_0 to Γ_5. Their roles are explained below and by the functional scheme in Figure 3.

The purpose of mapping $\Gamma_0 : \mathbb{R}^2 \to \mathbb{T}^N$ is to compute the reference shape trajectory

$$\boldsymbol{\beta}_r(t) = \Gamma_0(u_{Nr}(t)), \qquad (22)$$

respecting the S-P condition (14), as a bounded steady response of kinematics (13) upon a knowledge of the prescribed reference guidance velocity $u_{Nr}(t)$. The steady response $\boldsymbol{\beta}_r(t)$ computed as a solution of Equation (13) is guaranteed to be compatible with the reference guidance trajectory $q_{Nr}(t)$. Note that signal $\boldsymbol{\beta}_r(t)$ is computed only for the auxiliary purposes (needed by mappings Γ_1 and Γ_2, see Equations (23) and (24)) and will not be directly used by a control law.

Mapping $\Gamma_1 : \mathbb{R}^3 \times \mathbb{T}^N \to \mathbb{R}^3$ returns a reference posture for the tractor, i.e.

$$q_{0r} \equiv \bar{q}_{0r} = \Gamma_1(q_{Nr}, \boldsymbol{\beta}_r) \triangleq \text{inv}Q^0(q_{Nr}, \boldsymbol{\beta}_r), \qquad (23)$$

where $\text{inv}Q^0$ represents the inverse posture kinematics (8) for $i = 0$, evaluated here by taking as arguments the reference signals (see the direction of mapping Γ_1 denoted in Figure 1).

Mapping $\Gamma_2 : \mathbb{R}^2 \times \mathbb{T}^N \to \mathbb{R}^2$ computes a reference velocity for the tractor, i.e.

$$u_{0r} \equiv \bar{u}_{0r} = \Gamma_2(u_{Nr}, \boldsymbol{\beta}_r) \triangleq \text{inv}V^0(u_{Nr}, \boldsymbol{\beta}_r), \qquad (24)$$

where $\text{inv}V^0$ represents the inverse velocity kinematics (11) for $i = 0$, evaluated here by taking as arguments the reference signals (see the direction of mapping Γ_2 denoted in Figure 1).

Mapping $\Gamma_3 : \mathbb{R}^2 \to \mathbb{T}^N$ extracts a bounded steady response

$$\bar{\boldsymbol{\beta}}_r(t) = \Gamma_3(\bar{u}_{0r}(t)) \qquad (25)$$

of the reference virtual shape kinematics (cf. with Equation (13))

$$\dot{\bar{\boldsymbol{\beta}}}_r \overset{(3)}{=} \bar{S}_\beta(\bar{\boldsymbol{\beta}}_r)\bar{u}_{0r} \qquad (26)$$

upon a knowledge of reference input $\bar{u}_{0r} = [\bar{\omega}_{0r} \ \bar{v}_{0r}]^\top$ returned by mapping (24). Depending on the character of input $\bar{u}_{0r}$, the steady response $\bar{\boldsymbol{\beta}}_r(t)$ may be constant (computable in a closed form, see Appendix A1) or time-varying (for a non-trivial periodic reference input $\bar{u}_{0r}(t)$, the steady response $\bar{\boldsymbol{\beta}}_r(t)$ usually corresponds to a limit cycle in a shape space). Thus, in general, a bounded steady response of kinematics (26) can be extracted from its solution obtained by (numerical) integration of Equation (26). Note that $\bar{\boldsymbol{\beta}}_r$ is computed only for the auxiliary purposes (needed by mapping Γ_4, see Equation (27)) and will not be used directly during a control process.

Mapping $\mathbf{\Gamma}_4 : \mathbb{R}^3 \times \mathbb{T}^N \to \mathbb{R}^3$ returns a reference guidance trajectory for the virtual vehicle, i.e.

$$\bar{\boldsymbol{q}}_{Nr} = \mathbf{\Gamma}_4(\bar{\boldsymbol{q}}_{0r}, \bar{\boldsymbol{\beta}}_r) \triangleq \bar{\boldsymbol{Q}}^N(\bar{\boldsymbol{q}}_{0r}, \bar{\boldsymbol{\beta}}_r), \qquad (27)$$

where $\bar{\boldsymbol{Q}}^N$ represents the direct posture kinematics for the virtual vehicle determined by Equation (9) for $i = N$, and evaluated by taking as arguments the reference signals of the virtual vehicle (see the direction of mapping $\mathbf{\Gamma}_4$ denoted in Figure 1).

Mapping $\mathbf{\Gamma}_5 : \mathbb{R}^2 \times \mathbb{T}^N \to \mathbb{R}^2$ computes the reference guidance velocity $\bar{\boldsymbol{u}}_{Nr}$ for the last trailer of the virtual vehicle based on the reference velocity of the tractor $\bar{\boldsymbol{u}}_{0r} \equiv \boldsymbol{u}_{0r}$, i.e.

$$\bar{\boldsymbol{u}}_{Nr} = \mathbf{\Gamma}_5(\bar{\boldsymbol{u}}_{0r}, \bar{\boldsymbol{\beta}}_r) \triangleq \bar{\boldsymbol{V}}^N(\bar{\boldsymbol{u}}_{0r}, \bar{\boldsymbol{\beta}}_r), \qquad (28)$$

where $\bar{\boldsymbol{V}}^N$ represents the direct velocity kinematics for the virtual vehicle determined by Equation (10) for $i = 0$, evaluated here by taking as arguments the reference signals (see the direction of mapping $\mathbf{\Gamma}_5$ denoted in Figure 1).

Remark 3.4: The mapping $\mathbf{\Gamma}$ introduced in Equation (16) results from the following compositions (cf. Figure 3):

$$\mathbf{\Gamma}_q = \mathbf{\Gamma}_4 \left[\mathbf{\Gamma}_1(\boldsymbol{q}_{Nr}, \mathbf{\Gamma}_0(\boldsymbol{u}_{Nr})), \mathbf{\Gamma}_3(\mathbf{\Gamma}_2(\boldsymbol{u}_{Nr}, \mathbf{\Gamma}_0(\boldsymbol{u}_{Nr}))) \right],$$
$$\mathbf{\Gamma}_u = \mathbf{\Gamma}_5 \left[\mathbf{\Gamma}_2(\boldsymbol{u}_{Nr}, \mathbf{\Gamma}_0(\boldsymbol{u}_{Nr})), \mathbf{\Gamma}_3(\mathbf{\Gamma}_2(\boldsymbol{u}_{Nr}, \mathbf{\Gamma}_0(\boldsymbol{u}_{Nr}))) \right].$$

It is worth to stress that since we are interested only in the S-P reference trajectories $\boldsymbol{q}_r(t)$ for the forward motion conditions, the mapping $\mathbf{\Gamma}$ should preserve the S-P property and forward motion conditions for the virtual vehicle.

Remark 3.5: It can be easily shown that application of mapping $\mathbf{\Gamma}_u$ leads to the following implications:

$$\boldsymbol{u}_{Nr} = \text{const} \ \Rightarrow \ \bar{\boldsymbol{u}}_{Nr} = \text{const}, \qquad (29)$$
$$\| \boldsymbol{u}_{Nr} \| \leq \delta_1 \ \Rightarrow \ \| \bar{\boldsymbol{u}}_{Nr} \| \leq \eta_1 \delta_1 =: \bar{\delta}_1, \qquad (30)$$
$$\| \dot{\boldsymbol{u}}_{Nr} \| \leq \delta_2 \ \Rightarrow \ \| \dot{\bar{\boldsymbol{u}}}_{Nr} \| \leq (\eta_2 \delta_1 + \eta_3 \delta_2) =: \bar{\delta}_2, \qquad (31)$$

where the upper bounds δ_1, δ_2 have been introduced in (r2), while $\eta_1 > 0$ and $\eta_2, \eta_3 > 0$ are some finite constants.

4. Analysis of control performance in the closed-loop system

We are going to show asymptotic stability of point $(\tilde{\bar{\boldsymbol{\beta}}}, \bar{\boldsymbol{e}}_N) = (\boldsymbol{0}, \boldsymbol{0})$ for the virtual vehicle, and next we will prove that it entails asymptotic convergence of tracking errors $\tilde{\boldsymbol{\beta}}(t)$ and $\boldsymbol{e}_N(t)$ to zero for the real vehicle as $t \to \infty$. The first stability result can be immediately inferred upon Theorem 1 formulated in Michałek (2017) which allows claiming what follows.

Lemma 4.1 (Upon Theorem 1 from Michałek (2017))**:** *Assume the S-P reference trajectory $\boldsymbol{q}_r(t)$ satisfying (r1)–(r2) is given for the real vehicle, and the corresponding S-P reference trajectory $\bar{\boldsymbol{q}}_r(t)$ has been computed using mapping (16). Application of control law (19) into kinematics of the virtual N-trailer satisfying Assumptions A2–A3 guarantees local asymptotic stability of point $(\tilde{\bar{\boldsymbol{\beta}}}, \bar{\boldsymbol{e}}_N) = (\boldsymbol{0}, \boldsymbol{0})$ in some basin of attraction $\mathcal{D}_B \times \mathcal{D}_E$ when one of the two following conditions is met:*

(s1) $\bar{\boldsymbol{u}}_{Nr} = const$, or
(s2) $\bar{\boldsymbol{u}}_{Nr} = \bar{\boldsymbol{u}}_{Nr}(t)$ and $\forall \, t \geq 0$ $\| \bar{\boldsymbol{u}}_{Nr}(t) \| \leq \bar{\delta}_1, \| \dot{\bar{\boldsymbol{u}}}_{Nr}(t) \| \leq \bar{\delta}_2$
for sufficiently small constants $\bar{\delta}_1, \bar{\delta}_2 > 0$.

Proof: See the proof of Theorem 1 in Michałek (2017). □

The above lemma leads to the conclusion that the virtual N-trailer will asymptotically track the S-P reference trajectory $\bar{\boldsymbol{q}}_r(t)$ (mapped by $\mathbf{\Gamma}$ from the original S-P trajectory $\boldsymbol{q}_r(r)$) in the forward motion strategy when the virtual guidance velocity is constant, or when it is time-varying but the reference motion is sufficiently slow with the reference acceleration small enough. Recalling implications (29)–(31), it is evident that conditions (s1)–(s2) can be replaced with analogous conditions imposed on the reference velocity $\boldsymbol{u}_{Nr}$ defined for the real vehicle with the upper bounds $\delta_1 = \bar{\delta}_1/\eta_1$ and $\delta_2 = (\bar{\delta}_2 - \bar{\delta}_1 \eta_2/\eta_1)/\eta_3$.

Solution to the underlying Problem 2.1 is provided now by the following theorem.

Theorem 4.1: *Local asymptotic stability of point $(\tilde{\bar{\boldsymbol{\beta}}}, \bar{\boldsymbol{e}}_N) = (\boldsymbol{0}, \boldsymbol{0})$, guaranteed by Lemma 4.1, entails boundedness of tracking errors $\tilde{\boldsymbol{\beta}}(t), \boldsymbol{e}_N(t)$ for the real vehicle and their asymptotic convergence $\tilde{\boldsymbol{\beta}}(t) \to \boldsymbol{0}$ and $\boldsymbol{e}_N(t) \to \boldsymbol{0}$ as $t \to \infty$.*

Proof: Since $\| \bar{\boldsymbol{e}}_N \| < \infty$ (upon Lemma 4.1), then also $\| \bar{\boldsymbol{q}}_N \| = \| \bar{\boldsymbol{q}}_{Nr} - \bar{\boldsymbol{e}}_N \| < \infty$. As a consequence, a posture of the tractor $\| \boldsymbol{q}_0 \| \equiv \| \bar{\boldsymbol{q}}_0 \| = \| \text{inv} \bar{\boldsymbol{Q}}^0(\bar{\boldsymbol{q}}_N, \bar{\boldsymbol{\beta}}) \| < \infty$, and also $\| \boldsymbol{q}_N \| = \| \boldsymbol{Q}^N(\boldsymbol{q}_0, \boldsymbol{\beta}) \| < \infty$, which finally imply $\| \boldsymbol{q}_{Nr} - \boldsymbol{q}_N \| = \| \boldsymbol{e}_N \| < \infty$.

Furthermore, upon the relation (17) and using definitions (21) and (18) one can write the following equalities:

$$\bar{\boldsymbol{q}}_N = \bar{\boldsymbol{Q}}^N [\text{inv} \boldsymbol{Q}^0(\boldsymbol{q}_N, \boldsymbol{\beta}), \bar{\boldsymbol{\beta}}],$$
$$\bar{\boldsymbol{q}}_{Nr} - \bar{\boldsymbol{e}}_N = \bar{\boldsymbol{Q}}^N [\text{inv} \boldsymbol{Q}^0(\boldsymbol{q}_N, \boldsymbol{\beta}), \bar{\boldsymbol{\beta}}],$$
$$\bar{\boldsymbol{Q}}^N [\text{inv} \boldsymbol{Q}^0(\boldsymbol{q}_{Nr}, \boldsymbol{\beta}_r), \bar{\boldsymbol{\beta}}_r] - \bar{\boldsymbol{e}}_N = \bar{\boldsymbol{Q}}^N [\text{inv} \boldsymbol{Q}^0(\boldsymbol{q}_N, \boldsymbol{\beta}), \bar{\boldsymbol{\beta}}].$$

According to Lemma 4.1, we can write that terminally, for $(\tilde{\bar{\boldsymbol{\beta}}}, \bar{\boldsymbol{e}}_N) \to (\boldsymbol{0}, \boldsymbol{0})$, holds

$$\bar{\boldsymbol{Q}}^N [\text{inv} \boldsymbol{Q}^0(\boldsymbol{q}_{Nr}, \boldsymbol{\beta}_r), \bar{\boldsymbol{\beta}}_r] = \bar{\boldsymbol{Q}}^N [\text{inv} \boldsymbol{Q}^0(\boldsymbol{q}_N, \boldsymbol{\beta}), \bar{\boldsymbol{\beta}}_r]. \quad (32)$$

Since mapping $\bar{\boldsymbol{Q}}^N(\boldsymbol{a}, \boldsymbol{b})$ is diffeomorphic with respect to $\boldsymbol{a}$ for any fixed $\boldsymbol{b}$, one can infer that terminally, for $(\tilde{\bar{\boldsymbol{\beta}}}, \bar{\boldsymbol{e}}_N) \to (\boldsymbol{0}, \boldsymbol{0})$, Equation (32) implies

$$\text{inv} \boldsymbol{Q}^0(\boldsymbol{q}_{Nr}, \boldsymbol{\beta}_r) = \text{inv} \boldsymbol{Q}^0(\boldsymbol{q}_N, \boldsymbol{\beta}) \qquad (33)$$
$$\overset{(15)}{=} \text{inv} \boldsymbol{Q}^0(\boldsymbol{q}_{Nr} - \boldsymbol{e}_N, \boldsymbol{\beta}_r - \tilde{\boldsymbol{\beta}}). \qquad (34)$$

We will return to the above partial result later on.

Next, we are going to show that $\tilde{\boldsymbol{\beta}}(t)$ asymptotically tends to zero as $t \to \infty$. To this purpose, let us derive the shape-error dynamics of the real vehicle as follows:

$$\dot{\tilde{\boldsymbol{\beta}}} = \dot{\boldsymbol{\beta}}_r - \dot{\boldsymbol{\beta}} \overset{(3)}{=} \boldsymbol{S}_\beta(\boldsymbol{\beta}_r) \boldsymbol{u}_{0r} - \boldsymbol{S}_\beta(\boldsymbol{\beta}) \boldsymbol{u}_0, \qquad (35)$$

where $\boldsymbol{u}_{0r}(t)$ is the reference tractor velocity along the reference trajectory $\boldsymbol{q}_r(t)$. Introducing the control input error

$$\tilde{\boldsymbol{u}}_0 \triangleq \boldsymbol{u}_{0r} - \boldsymbol{u}_0 \overset{(19)}{=} \boldsymbol{u}_{0r} - \prod_{j=1}^{N} \bar{\boldsymbol{J}}_j^{-1}(\bar{\beta}_j)\boldsymbol{\phi}(\bar{\boldsymbol{e}}_N, t)$$

$$= \prod_{j=1}^{N} \bar{\boldsymbol{J}}_j^{-1}(\bar{\beta}_{jr})\bar{\boldsymbol{u}}_{Nr} - \prod_{j=1}^{N} \bar{\boldsymbol{J}}_j^{-1}(\bar{\beta}_{jr} - \tilde{\beta}_j)\boldsymbol{\phi}(\bar{\boldsymbol{e}}_N, t) \quad (36)$$

we can rewrite Equation (35) as

$$\dot{\tilde{\boldsymbol{\beta}}} = \boldsymbol{S}_\beta(\boldsymbol{\beta}_r)\boldsymbol{u}_{0r} - \boldsymbol{S}_\beta(\boldsymbol{\beta}_r - \tilde{\boldsymbol{\beta}})[\boldsymbol{u}_{0r} - \tilde{\boldsymbol{u}}_0]$$

$$= \underbrace{\boldsymbol{S}_\beta(\boldsymbol{\beta}_r)\boldsymbol{u}_{0r} - \boldsymbol{S}_\beta(\boldsymbol{\beta}_r - \tilde{\boldsymbol{\beta}})\boldsymbol{u}_{0r}}_{f(\tilde{\boldsymbol{\beta}}, t)} + \underbrace{\boldsymbol{S}_\beta(\boldsymbol{\beta}_r - \tilde{\boldsymbol{\beta}})\tilde{\boldsymbol{u}}_0}_{g(\tilde{\boldsymbol{\beta}}, \tilde{\boldsymbol{u}}_0, t)} \quad (37)$$

where

$$\dot{\tilde{\boldsymbol{\beta}}} = \boldsymbol{f}(\tilde{\boldsymbol{\beta}}, t) \quad (38)$$

represents the *nominal* shape-error dynamics, while $\boldsymbol{g}(\tilde{\boldsymbol{\beta}}, \tilde{\boldsymbol{u}}_0, t)$ is a perturbation term with perturbing input $\tilde{\boldsymbol{u}}_0$, such that, in general, $\boldsymbol{g}(\boldsymbol{0}, \tilde{\boldsymbol{u}}_0, t) \not\equiv \boldsymbol{0}$. By recalling the definition (36), the form of matrix $\bar{\boldsymbol{J}}_i^{-1}(\bar{\beta}_i)$, properties (p1)–(p3) of function $\boldsymbol{\phi}$, and due to boundedness and asymptotic convergence of errors $\tilde{\tilde{\boldsymbol{\beta}}}$ and $\bar{\boldsymbol{e}}_N$ guaranteed by Lemma 4.1, one may observe that

(u1) $\forall t \geq 0 \; \|\tilde{\boldsymbol{u}}_0(\tilde{\tilde{\boldsymbol{\beta}}}(t), \bar{\boldsymbol{e}}_N(t), t)\| < \infty, \|\tilde{\boldsymbol{u}}_0(\boldsymbol{0}, \boldsymbol{0}, t)\| \equiv 0,$

(u2) $\|\tilde{\boldsymbol{u}}_0(\tilde{\tilde{\boldsymbol{\beta}}}(t), \bar{\boldsymbol{e}}_N(t), t)\| \to 0$ as $t \to \infty$.

It can be shown (see Appendix A2) that the equilibrium point $\tilde{\boldsymbol{\beta}} = \boldsymbol{0}$ of the nominal shape-error dynamics (38) is locally exponentially stable during forward tracking of the S-P reference trajectories corresponding to the virtual reference velocity satisfying (s1) or (s2) stated in Lemma 4.1. Thus, according to the Converse Lyapunov Theorem (Khalil, 2002), for some basin of attraction $\mathcal{D}_b = \{\tilde{\boldsymbol{\beta}} \in \mathbb{R}^N : \|\tilde{\boldsymbol{\beta}}\| < r_b\}$, $r_b > 0$, there exists a continuously differentiable function $V(\tilde{\boldsymbol{\beta}}, t) : \mathcal{D}_b \times [0, \infty) \to \mathbb{R}_{\geq 0}$ satisfying: $c_1\|\tilde{\boldsymbol{\beta}}\|^2 \leq V(\tilde{\boldsymbol{\beta}}, t) \leq c_2\|\tilde{\boldsymbol{\beta}}\|^2$, $(\partial V/\partial t) + (\partial V/\partial\tilde{\boldsymbol{\beta}})\boldsymbol{f}(\tilde{\boldsymbol{\beta}}, t) \leq -c_3\|\tilde{\boldsymbol{\beta}}\|^2$, and $\|\partial V/\partial\tilde{\boldsymbol{\beta}}\| \leq c_4\|\tilde{\boldsymbol{\beta}}\|$ for some positive constants c_i, $i = 1, 2, 3, 4$. For the perturbed shape-error dynamics (37) one can assess the time derivative of function V as follows:

$$\dot{V} = \frac{\partial V}{\partial t} + \frac{\partial V}{\partial\tilde{\boldsymbol{\beta}}}[\boldsymbol{f}(\tilde{\boldsymbol{\beta}}, t) + \boldsymbol{g}(\tilde{\boldsymbol{\beta}}, \tilde{\boldsymbol{u}}_0, t)]$$

$$\leq -c_3\|\tilde{\boldsymbol{\beta}}\|^2 + \left\|\frac{\partial V}{\partial\tilde{\boldsymbol{\beta}}}\right\| \|\boldsymbol{g}(\tilde{\boldsymbol{\beta}}, \tilde{\boldsymbol{u}}_0, t)\|$$

$$\leq -c_3\|\tilde{\boldsymbol{\beta}}\|^2 + c_4\delta_s\|\tilde{\boldsymbol{\beta}}\|\,\|\tilde{\boldsymbol{u}}_0\| + \mu c_3\|\tilde{\boldsymbol{\beta}}\|^2 - \mu c_3\|\tilde{\boldsymbol{\beta}}\|^2$$

$$= -c_3(1 - \mu)\|\tilde{\boldsymbol{\beta}}\|^2 + \|\tilde{\boldsymbol{\beta}}\|\left[c_4\delta_s\|\tilde{\boldsymbol{u}}_0\| - \mu c_3\|\tilde{\boldsymbol{\beta}}\|\right], \quad (39)$$

where $\mu \in (0, 1)$ is a majorisation constant, while the assessment $\|\boldsymbol{g}(\tilde{\boldsymbol{\beta}}, \tilde{\boldsymbol{u}}_0, t)\| \leq \|\boldsymbol{S}_\beta(\boldsymbol{\beta}_r - \tilde{\boldsymbol{\beta}})\| \|\tilde{\boldsymbol{u}}_0\| \leq \delta_s\|\tilde{\boldsymbol{u}}_0\|$ results from Equation (37) and the form of matrix $\boldsymbol{S}_\beta$ (cf. Equation

(3)). Upon Equation (39), we can conclude that

$$\dot{V} \leq -c_3(1 - \mu)\|\tilde{\boldsymbol{\beta}}\|^2 \quad \text{for} \quad \|\tilde{\boldsymbol{\beta}}\| \geq \underbrace{\frac{c_4\delta_s}{c_3\mu}\|\tilde{\boldsymbol{u}}_0\|}_{\sigma(\|\tilde{\boldsymbol{u}}_0\|)} \quad (40)$$

where $\sigma(\|\tilde{\boldsymbol{u}}_0\|)$ is a function of class $\mathcal{K}$. Thus, the perturbed dynamics (37) is Locally Input-to-State Stable (LISS) (Khalil, 2002; Isidori, 1999; Teel, 1996). As a consequence, a solution of Equation (37) satisfies

$$\forall t \geq 0 \quad \|\tilde{\boldsymbol{\beta}}(t)\| \leq \max\left\{\rho(\|\tilde{\boldsymbol{\beta}}(0)\|, t); \gamma\left(\sup_{t\geq 0}\|\tilde{\boldsymbol{u}}_0(t)\|\right)\right\}$$

for some $\mathcal{KL}$-class function ρ and the $\mathcal{K}$-class function $\gamma(\|\tilde{\boldsymbol{u}}_0\|) = \sqrt{c_2/c_1}\frac{c_4\delta_s}{c_s\mu}\|\tilde{\boldsymbol{u}}_0\|$ if

(c1) $\|\tilde{\boldsymbol{\beta}}(0)\| < r_b\sqrt{c_1/c_2}$, and

(c2) $\sup_{t\geq 0}\|\tilde{\boldsymbol{u}}_0(\tilde{\tilde{\boldsymbol{\beta}}}(t), \bar{\boldsymbol{e}}_N(t), t)\| < r_b\sqrt{c_1/c_2}\frac{c_3\mu}{c_4\delta_s}$.

According to definition (36) and properties (u1)–(u2), satisfaction of condition (c2) essentially depends on the tracking errors $\tilde{\tilde{\boldsymbol{\beta}}}$, $\bar{\boldsymbol{e}}_N$, and on properties of control function $\boldsymbol{\phi}(\bar{\boldsymbol{e}}_N, t)$. In particular, if locally for $(\tilde{\tilde{\boldsymbol{\beta}}}, \bar{\boldsymbol{e}}_N) \in \mathcal{D}_B \times \mathcal{D}_E$ the following domination holds $\|\tilde{\boldsymbol{u}}_0(\tilde{\tilde{\boldsymbol{\beta}}}, \bar{\boldsymbol{e}}_N, t)\| \leq \kappa(\|[\tilde{\tilde{\boldsymbol{\beta}}}^\top \; \bar{\boldsymbol{e}}_N^\top]\|)$, where $\kappa(\cdot)$ is a function of class $\mathcal{K}$, then (c2) can be replaced by a condition formulated directly with respect to the tracking errors, i.e.

(c2) $\sup_{t\geq 0}\|[\tilde{\tilde{\boldsymbol{\beta}}}^\top(t) \; \bar{\boldsymbol{e}}_N^\top(t)]\| < \kappa^{-1}\left(r_b\sqrt{c_1/c_2}\frac{c_3\mu}{c_4\delta_s}\right)$.

Furthermore, according to the asymptotic gain property (Isidori, 1999) one can write for the LISS dynamics (37)

$$\limsup_{t\to\infty}\|\tilde{\boldsymbol{\beta}}(t)\| \leq \gamma\left(\limsup_{t\to\infty}\|\tilde{\boldsymbol{u}}_0(\tilde{\tilde{\boldsymbol{\beta}}}(t), \bar{\boldsymbol{e}}_N(t), t)\|\right) \overset{(u2)}{=} 0.$$
$$(41)$$

Now, we shall return to the result denoted by (33) and (34). Since for any fixed $\boldsymbol{b}$ the mapping $\text{inv}\boldsymbol{Q}^0(\boldsymbol{a}, \boldsymbol{b})$ is diffeomorphic with respect to $\boldsymbol{a}$, the asymptotic convergence of $\tilde{\boldsymbol{\beta}}$ to zero inferred upon Equation (41) allows one to conclude that satisfaction of Equations (33) and (34) for $\tilde{\boldsymbol{\beta}}(t) \to \boldsymbol{0}$ must entail $\boldsymbol{e}_N(t) \to \boldsymbol{0}$ as $t \to \infty$. □

5. Numerical and experimental results

5.1 Numerical validation

We present exemplary results of tracking a complex reference trajectory obtained for the nS3T kinematics ($N = 3$) characterised by trailer lengths $L_i = 0.25$ m, ($i = 1, 2, 3$) and hitching offsets $L_{h1} = L_{h3} = 0.05$ m, $L_{h2} = -0.05$ m (mixed signs of hitching offsets). A reference trajectory $\boldsymbol{q}_r(t)$ was computed in four main steps. In the first step, the four way-points (θ_{wp}, x_{wp}, y_{wp}) defining the desired orientation, θ_{wp}, and the desired position coordinates (x_{wp}, y_{wp}) of the last trailer were chosen as
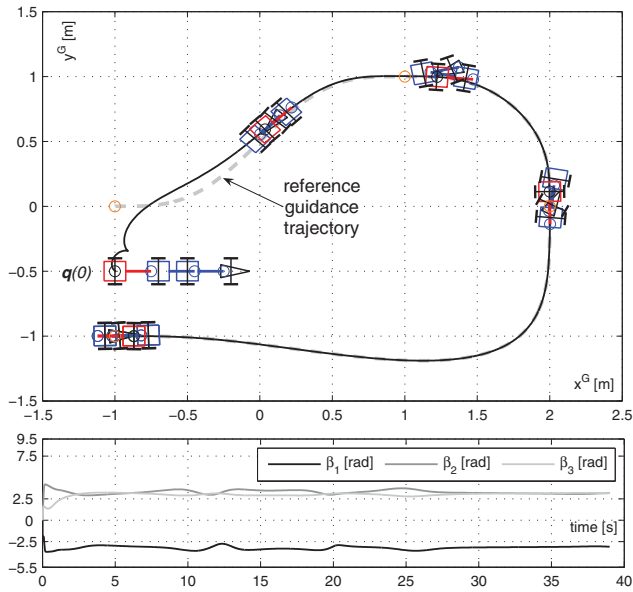
Figure 4. Simulation results of forward tracking the complex reference trajectory with direct application of the control law proposed in Michałek (2017) to the nS3T kinematics with mixed signs of hitching offsets illustrating the jackknife effect in vehicle joints (an initial condition of the vehicle has been denoted by $q(0)$).

follows: $(0, -1, 0)$, $(0, 1, 1)$, $(-\frac{\pi}{2}, 2, 0)$ and $(-\pi, -1, -1)$, all expressed in $([rad],[m],[m])$, respectively. Next, three 7th degree polynomials were continuously concatenated at the successive way-points in order to establish preliminary reference guidance trajectory $q_{Nr}(\tau)$ compatible with kinematics (12) for $\tau \in [0, T)$, with $T > 0$ being a prescribed time-horizon. In the third step, the corresponding reference shape trajectory $\beta_r(\tau)$ avoiding the jackknife effect was computed taking into account kinematics (13) together with constraint (14). Finally, the reference trajectory $q_r(t)$ was obtained from $q_{rN}(\tau)$ and $\beta_r(\tau)$ by applying an appropriate time scaling to guarantee a constant reference longitudinal velocity $v_{Nr} = 0.2$ m/s within the whole control time-horizon. Values of the trailers' lengths for the virtual vehicle were set as $\bar{L}_i = 0.5L_i = 0.125$ m for $i = 1, 2, 3$, while hitching offsets were set (upon A2) to $\bar{L}_{hi} = -0.05$ m for $i = 1, 2, 3$ ($h_i = 1$). The unicycle controller proposed in Canudas de Wit et al. (1996) was applied in the outer loop of a cascade from Figure 2 resulting in the control function

$$\phi(\bar{e}_N, t) \triangleq \begin{bmatrix} \bar{\omega}_{Nr} + k_0\bar{v}_{Nr}\tilde{e}_3 s\bar{e}_\theta/\bar{e}_\theta + k_1(\bar{u}_{Nr})\bar{e}_\theta \\ \bar{v}_{Nr}c\bar{e}_\theta + k_2(\bar{u}_{Nr})\tilde{e}_2 \end{bmatrix}, \quad (42)$$

where $\tilde{e}_2 = \bar{e}_x c\bar{\theta}_N + \bar{e}_y s\bar{\theta}_N$ and $\tilde{e}_3 = -\bar{e}_x s\bar{\theta}_N + \bar{e}_y c\bar{\theta}_N$, $k_0 > 0$ is a design parameter (taken as $k_0 = 10$), while $k_1(\bar{u}_{Nr}) = k_2(\bar{u}_{Nr}) \triangleq 2\sqrt{\bar{\omega}_{Nr}^2 + k_0\bar{v}_{Nr}^2}$ are the positive definite functions. All the simulations were conducted in the Matlab–Simulink environment using the *ode45* solver.

First, let us illustrate the consequences of applying the cascade-like controller originally proposed in Michałek (2017) to the considered nS3T vehicle with mixed signs of hitching offsets. The results of numerical simulations have been presented in Figure 4. Although the guidance segment asymptotically tracks the reference trajectory, the joint angles evolve around the values of $\pm\pi$; one observes a complete folding of a vehicle in its joints,
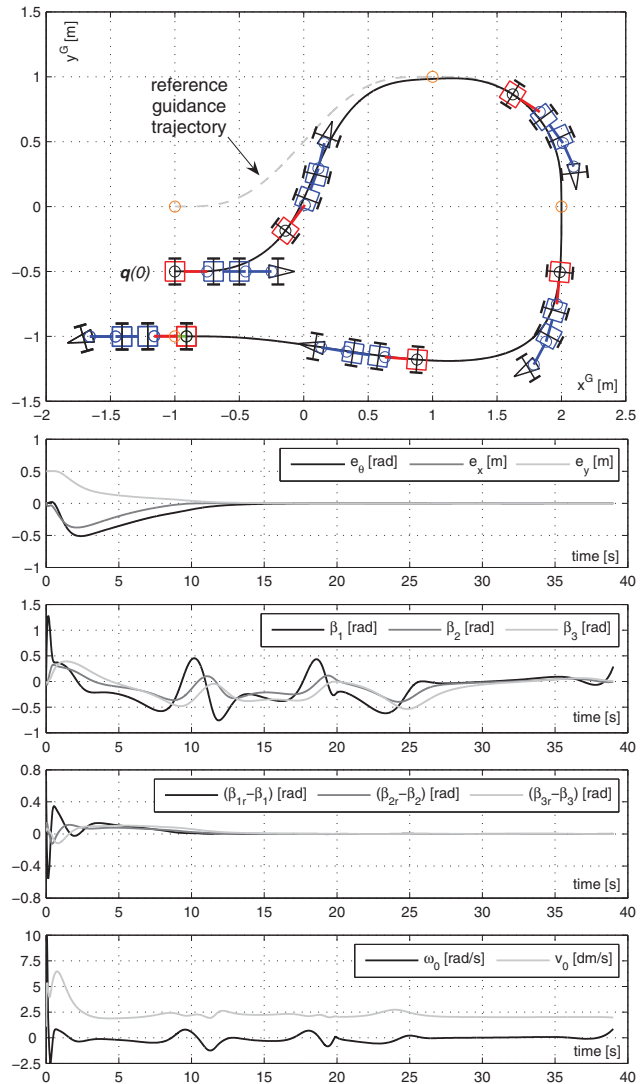
Figure 5. Simulation results of forward tracking the complex reference trajectory obtained for a nS3T kinematics with mixed signs of hitching offsets (an initial condition of the vehicle has been denoted by $q(0)$).

corresponding to the jackknife effect, which in practical applications usually leads to a damage of a mechanical construction. This effect is a direct consequence of the non-minimum-phase vehicle's kinematics.

Next, let us show improvement in realisation of the same task using the control law defined by Equation (19). The results of simulations conducted with the controller (19) are presented in Figure 5. It is worth noting that the vehicle does not experience any jackknife effect and moves smoothly during a control process despite a non-minimum-phase property of its kinematics in the considered motion conditions. The joint angles evolve in this case around the zero value. A smooth evolution of control signals, away of a short initial picking in the case of angular velocity $\omega_0(t)$ (not shown in the plot for the sake of presentation clarity) looks promising in the context of practical applications of the control strategy. Note that the resultant terminal tracking accuracy essentially depends on a precision of computing the mappings Γ_0 and Γ_3. In the case of perfect computations of Γ_0 and Γ_3 one should expect the asymptotic convergence of tracking errors to zero.
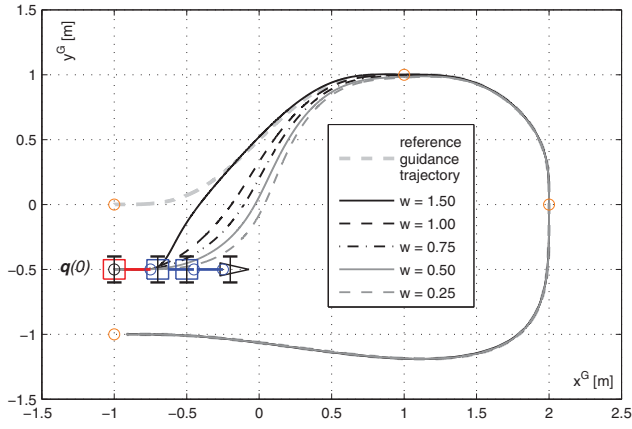
Figure 6. Influence of trailers' lengths $\bar{L}_i = w \cdot L_i$ of the virtual vehicle on the transient control performance for various values of scaling factor w (an initial condition of the vehicle has been denoted by $\boldsymbol{q}(0)$).
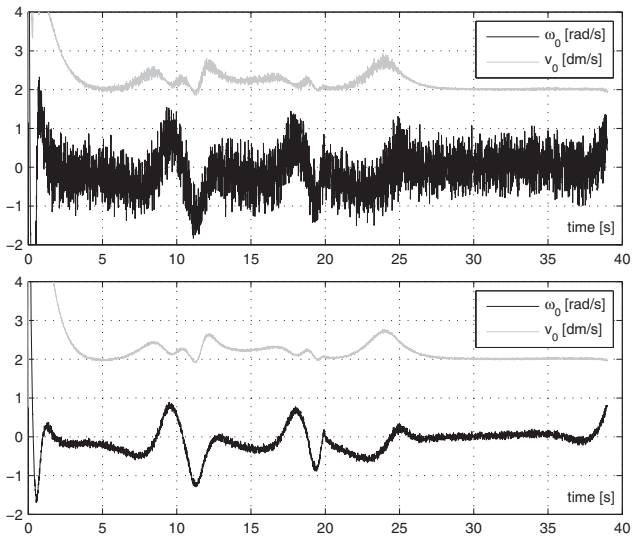
Figure 7. Control signals obtained in the closed-loop system illustrating a change in sensitivity to a feedback noise for two selected values of design factors h_i introduced in Assumption A2: $h_i = 1$ (the upper plot) and $h_i = 2$ (the bottom plot), $i = 1, 2, 3$.

Figure 6 illustrates an influence of the virtual vehicle's kinematic parameters $\bar{L}_i$ on the transient control performance obtained with the outer-loop control function (42). Upon the plot, one can conclude that selection of virtual trailers' lengths $\bar{L}_i := w \cdot L_i$ with larger values of scaling factor $w > 0$ generally implies faster convergence of a tracking error for the real vehicle. The price is, however, a higher control cost observed in the transient stage.

According to Assumptions A1 and A2, one has to limit application of the proposed cascade-like controller solely to N-trailers with off-axle hitching. It is a direct consequence of the form of control law (19), where the inverse matrices $\bar{\boldsymbol{J}}_i^{-1}$ are well determined only for $\bar{L}_{hi} \neq 0$. For the non-zero but very short offsets L_{hi} the inverse matrices in Equation (19), although formally well defined, may cause in practice substantial amplification of measurement noises corrupting the outer feedback loop. The plots presented in Figure 7 reveal how the design factors h_i introduced in Assumption A2 help in decreasing the noise sensitivity of the closed-loop system. For this purpose, the uniformly

Figure 8. View of the laboratory-scale N-trailer vehicle used in the experiments.

distributed random noises from the range $[-0.002; 0.002]$ were added in a feedback loop to components of configuration vector $\boldsymbol{q}_N$. All other simulation conditions were left unchanged, except $\bar{L}_i = L_i$. The upper plot in Figure 7 illustrates the control signals obtained for factors $h_i = 1, i = 1, 2, 3$, while the bottom plot corresponds to factors $h_i = 2, i = 1, 2, 3$. The control quality for the two mentioned control scenarios was evaluated by the steady-motion integral $J \triangleq \int_{t_1}^{t_2} \| \boldsymbol{e}_N(t) \| \, dt$, with $t_1 = 20$ s and $t_2 = 39$ s, obtaining $J = 0.0201$ for $h_i = 1$ and $J = 0.0143$ for $h_i = 2$. One observes a clear beneficial effect of control smoothing achieved with longer offsets $\bar{L}_{hi}$, corresponding to even slightly better average tracking accuracy reflected by a smaller value of integral J obtained for $h_i = 2$.

5.2 Experimental verification

Experimental trials were performed on the laboratory testbed equipped with the three-trailer ($N = 3$) vehicle presented in Figure 8. Kinematic parameters of the vehicle were $L_i = 0.229$ m and $L_{hi} = 0.048$ m for $i = 1, 2, 3$. The proposed control system was implemented on the vehicle's board using a floating-point digital signal processor. An external vision system (connected with the vehicle by a radio link) was used for estimation of the last trailer posture $\boldsymbol{q}_N$ to close the outer feedback loop. The angles β_i were measured by the absolute 14-bit encoders mounted in the vehicle's joints. The working frequency of the control system was equal to 100 Hz. The time-response of virtual shape kinematics was computed on-line according to Equation (20) by numerical integration after using the Euler-forward discretisation method. To address practical limitations resulting from the maximal admissible velocity $\omega_{\max} = 6$ rad/s of the tractor's wheels, the following velocity scaling procedure was applied in the input channel of the real vehicle:

$$\boldsymbol{u}_{0s}(t) = \begin{bmatrix} \omega_{0s}(t) \\ v_{0s}(t) \end{bmatrix} \triangleq s(t) \cdot \boldsymbol{u}_0(t) = \begin{bmatrix} s(t)\omega_0(t) \\ s(t)v_0(t) \end{bmatrix}, \quad (43)$$

where $s(t)$ is a scaling function

$$s(t) \triangleq \left[\max \left\{ 1; \frac{|\omega_{R0}(t)|}{\omega_{\max}}; \frac{|\omega_{L0}(t)|}{\omega_{\max}} \right\} \right]^{-1} \in (0, 1],$$

while $\omega_{R0} = (v_0 + 0.5b\omega_0)/r$ and $\omega_{L0} = (v_0 - 0.5b\omega_0)/r$ are the angular velocities of the tractor's wheels computed upon the components of $\boldsymbol{u}_0$ and using the tractor's wheel radius $r =$

Figure 9. Experimental results of forward tracking the complex periodic reference trajectory obtained using the laboratory-scale vehicle of nS3T kinematics with positive hitching offsets (an initial condition of the vehicle has been denoted by $q(0)$).

implemented in the outer loop of the vehicle's onboard control system. Parameters of the virtual vehicle were chosen in this case as $\bar{L}_i = 0.5 L_i = 0.1145$m and (according to Assumption A2) $\bar{L}_{hi} = -0.048$ m ($h_i = 1$) for $i = 1, 2, 3$.

Selected results of the conducted experimental trials are illustrated in Figure 9. Similarly as in the numerical tests, the terminal tracking accuracy obtainable in practice substantially depends on a numerical precision and sampling frequency with which the reference signals $\bar{q}_{Nr}$ and $\bar{u}_{Nr}$ are computed for the virtual vehicle. A small non-zero vicinity-tube, within which the terminal tracking errors evolve (seen in Figure 9), is also a consequence of small bounded slip/skid effects affecting the vehicles' wheels, the presence of a measurement noise corrupting a feedback loop, and unavoidable uncertainties of a mechanical construction of the experimental vehicle.

6. Concluding remarks

The cascade-like modular control law proposed in the paper is (to our best knowledge) the first control solution which allows the robotic vehicles of nSNT kinematics with positive or mixed-sign hitching offsets to asymptotically track complex reference trajectories (i.e. those with a varying curvature) in forward motion conditions for a case where the guidance point is located on the (last) trailer. Thanks to the cascade-like structure of the controller, one obtains high scalability of the solution, where a change of a number of trailers requires only a change of a number of matrix multiplications performed in the inner loop of the controller. A possible difficulty with application of the proposed *virtual-vehicle approach* may come from the need of a sufficient precision in computations of mappings Γ_0 and Γ_3, and in particular from finding the S-P reference trajectory for the real vehicle which is not a differentially flat system. The latter problem is interesting by itself and, we believe, deserves a wider discussion in a separate publication.

Disclosure statement

No potential conflict of interest was reported by the authors.

ORCID

Maciej Marcin Michałek http://orcid.org/0000-0002-9953-703X
Dariusz Pazderski http://orcid.org/0000-0002-8732-7350

References

Aguiar, A. P., Hespanha, J. P., & Kokotović, P. (2008). Performance limitations in reference-tracking and path-following for nonlinear systems. *Automatica, 44*(3), 598–610.
Astolfi, A., Bolzern, P., & Locatelli, A. (2004). Path-tracking of a tractor-trailer vehicle along rectilinear and circular paths: A Lyapunov-based approach. *IEEE Transactions on Robotics and Automation, 20*(1), 154–160.

0.029 m and the tractor's wheels base $b = 0.15$ m. Note that physically admissible control signal $\boldsymbol{u}_{0s}(t)$ commanded to the tractor preserves an instantaneous motion curvature determined by original components of $\boldsymbol{u}_0 = [\omega_0 \, v_0]^\top$ computed upon the control law (19).

In the sequel, we present the results of tracking a reference trajectory $\boldsymbol{q}_r(t)$ corresponding to the periodic guidance positional trajectory of a varying curvature where

$$x_{Nr}(p(t)) \triangleq \varpi(p(t)) \sin(2\pi \cdot p(t) + \pi),$$

$$y_{Nr}(p(t)) \triangleq \varpi(p(t)) \sin(2\pi \cdot p(t) + \pi/2),$$

and $\varpi(p(t)) = 0.12\cos(6\pi \cdot p(t)) + 0.8$, while the parameter $p(t)$ was computed by numerically solving the differential equation $\dot{p} = v_{Nr}/\sqrt{(\partial x_{Nr}/\partial p)^2 + (\partial y_{Nr}/\partial p)^2}$ for the initial condition $p(0) = 0$ in order to obtain a constant reference velocity $v_{Nr} = 0.05$ m/s along the guidance trajectory. The same control function $\boldsymbol{\phi}(\bar{\boldsymbol{e}}_N, t)$ used previously in Section 5.1 was

Auat Cheein, F. A., Scaglia, G., Torres-Torriti, M., Guivant, J., Prado, A. J., Arno, J., ...Rosell-Polo, J. R. (2016). Algebraic path tracking to aid the manual harvesting of olives using an automated service unit. *Biosystems Engineering, 142*, 117–132.

Backman, J., Oksanen, T., & Visala, A. (2012). Navigation system for agricultural machines: Nonlinear model predictive path tracking. *Computers and Electronics in Agriculture, 82*, 32–43.

Bolzern, P., DeSantis, R. M., & Locatelli, A. (2001). An input-output linearization approach to the control of an n-body articulated vehicle. *ASME Journal of Dynamic Systems, Measurement, and Control, 123*, 309–316.

Bolzern, P., DeSantis, R. M., Locatelli, A., & Masciocchi, D. (1998). Path-tracking for articulated vehicles with off-axle hitching. *IEEE Transactions on Control Systems Technology, 6*(4), 515–523.

Bullo, F., & Murray, R. M. (1996). Experimental comparison of trajectory trackers for a car with trailers. In J. Gertler, J. B. Cruz Jr., & M. Peshkin (Eds.) *Proceedings of the 1996 IFAC 13th world congress, 30 June-5 July* (pp. 407–412). San Francisco, USA: Elsevier.

Canudas de Wit, C., Siciliano, B., & Bastin, G. (1996). *Theory of robot control*. New York, NY: Springer-Verlag.

Cariou, C., Lenain, R., Thuilot, B., & Martinet, P. (2010). Path following of a vehicle-trailer system in presence of sliding: Application to automatic guidance of a towed agricultural implement. In R. C. Luo & H. Asama (Eds.) *Proceedings of the 2010 IEEE/RSJ IROS* (pp. 4976–4981). Taipei, Taiwan: IEEE.

Cheng, J., Wang, B., Zhang, Y., & Wang, Z. (2017). Backward orientation tracking control of mobile robot with N trailers. *International Journal of Control, Automation and Systems, 15*(X), 1–8.

Chiu, J., & Goswami, A. (2014). The critical hitch angle for jackknife avoidance during slow backing up of vehicle-trailer systems. *Vehicle System Dynamics, 52*(7), 992–1015.

Chung, W., Park, M., Yoo, K., Roh, J. I., & Choi, J. (2011). Backward-motion control of a mobile robot with *n* passive off-hooked trailers. *Journal of Mechanical Science and Technology, 25*(11), 2895–2905.

DeSantis, R. M., Bourgeot, J. M., Todeschi, J. N., & Hurteau, R. (2002). Path-tracking for tractor-trailers with hitching of both the on-axle and the off-axle kind. In C. DeSilva & F. Karray (Eds.) *Proceedings of the 2002 IEEE international symposium on intelligence control* (pp. 206–211). Vancouver, Canada: IEEE.

Hoagg, J. B., & Bernstein, D. S. (2007). Nonminimum-phase zeros. Much to do about nothing. *IEEE Control Systems Magazine, 27*(3), 45–57.

Isidori, A. (1999). *Nonlinear control systems II*. London: Springer.

Karkee, M., & Steward, B. L. (2010). Study of the open and closed loop characteristics of a tractor and a single axle towed implement system. *Journal of Terramechanics, 47*, 379–393.

Kayacan, E., Ramon, H., & Saeys, W. (2016). Robust trajectory tracking error model-based predictive control for unmanned ground vehicles. *IEEE/ASME Transactions on Mechatronics, 21*(2), 806–814.

Khalaji, A. K., & Moosavian, S. A. A. (2014). Robust adaptive controller for a tractor-trailer mobile robot. *IEEE/ASME Transaction on Mechatronics, 19*(3), 943–953.

Khalaji, A. K., & Moosavian, S. A. A. (2016). Dynamic modeling and tracking control of a car with *n* trailers. *Multibody System Dynamics, 37*, 211–225.

Khalil, H. K. (2002). *Nonlinear systems* (3rd ed.). Upper Saddle River, NJ: Prentice-Hall.

Kim, D., & Oh, J. (2002). Globally asymptotically stable tracking control for a trailer system. *Journal of Robotic Systems, 19*(5), 199–205.

Lamiraux, F., Sekhavat, S., & Laumond, J. (1999). Motion planning and control for Hilare pulling a trailer. *IEEE Transactions on Robotics and Automation, 15*(4), 640–652.

Leng, Z., & Minor, M. A. (2017). Curvature-based ground vehicle control of trailer path following considering sideslip and limited steering actuation. *IEEE Transactions on Intelligent Transportation Systems, 18*(2), 332–348.

Lizarraga, D., Morin, P., & Samson, C. (2001). Chained form approximation of a driftless system. Application to the exponential stabilization of the general N-trailer system. *International Journal of Control, 74*(16), 1612–1629.

Ma, B.-L., Niu, Y., Xie, W.-J., & Lin, S. (2014). Asymptotic path following control of tractor-trailers with off-axle hitching. In *Proceedings of the 2014 IEEE Chinese guidance, navigation and control conference* (pp. 2407–2412). Yantai: IEEE.

Martinez, J. L., Morales, J., Mandow, A., & Garcia-Cerezo, A. (2008). Steering limitations for a vehicle pulling passive trailers. *IEEE Transactions on Control Systems Technology, 16*(4), 809–818.

Michałek, M. (2013). Non-minimum-phase property of N-trailer kinematics resulting from off-axle interconnections. *International Journal of Control, 86*(4), 740–758.

Michałek, M. M. (2017). Cascade-like modular tracking controller for non-Standard N-Trailers. *IEEE Transactions on Control Systems Technology, 25*(2), 619–627.

Morin, P., & Samson, C. (2008a). Motion control of wheeled mobile robots. In B. Siciliano & O. Khatib (Eds.) *Springer handbook of robotics* (pp. 799–826). Berlin: Springer.

Morin, P., & Samson, C. (2008b). Transverse function control of a class of non-invariant driftless systems. Application to vehicles with trailers. In C. T. Abdallah & T. Parisini (Eds.) *Proceedings of the 47th IEEE conference on decision and control* (pp. 4312–4319). Cancun, Mexico: IEEE.

Pazderski, D., Waśkowicz, D., & Kozłowski, K. (2015). Motion control of vehicles with trailers using transverse function approach. Controller properties analysis. *Journal of Intelligent and Robotic Systems, 77*(3–4), 457–479.

Pradalier, C., & Usher, K. (2008). Robust trajectory tracking for a reversing tractor trailer. *Journal of Field Robotics, 25*(6–7), 378–399.

Rouchon, P., Fliess, M., Levine, J., & Martin, P. (1993). Flatness, motion planning and trailer systems. In R. A. DeCarlo & P. Ramadge (Eds.) *Proceedings of the 32nd conference on decision and control* (pp. 2700–2705). San Antonio, Texas: IEEE.

Seron, M. M., Braslavsky, J. H., & Goodwin, G. C. (1997). *Fundamental limitations in filtering and control*. London: Springer-Verlag.

Tan, H.-S., & Huang, J. (2014). Design of a high-performance automatic steering controller for bus revenue service based on how drivers steer. *IEEE Transactions on Robotics, 30*(5), 1137–1147.

Teel, A. R. (1996). A nonlinear small gain theorem for the analysis of control systems with saturation. *IEEE Transactions on Automatic Control, 41*(9), 1256–1270.

Werner, R., Kormann, G., & Mueller, S. (2013). Systematic model based path tracking control of actively steered implements in simulation and experiment. In A. Visala (Ed.) *Proceedings of the 4th IFAC conference on modelling and control in agriculture* (pp. 85–90). Espoo, Finland: Elsevier Science Direct - IFAC PapersOnline 2014.

Yuan, J., & Huang, Y. (2006). Path following control for tractor-trailer mobile robots with two kinds of connection structures. In Y. Lu & N. Xi (Eds.) *Proceedings of the 2006 IEEE/RSJ International Conference on Intelligent Robots and Systems* (pp. 2533–2538). Beijing, China: IEEE/RSJ.

Yuan, H., & Zhu, H. (2016). Anti-jackknife reverse tracking control of articulated vehicles in the presence of actuator saturation. *Vehicle System Dynamics, 54*(10), 1428–1447.

Yue, M., Hou, X., Gao, R., & Chen, J. (2018). Trajectory tracking control for tractor-trailer vehicles: A coordinated control approach. *Nonlinear Dynamics, 91*(2), 1061–1074.

Zhu, J. J. (1993). A note on extension of the eigenvalue concept. *IEEE Control Systems, 13*(6), 68–70.

Appendix

A1. Closed-form solution of Equation (26) for $\bar{u}_{0r} = [\bar{\omega}_{0r} \ \bar{v}_{0r}]^\top = const$

In the special case of a constant reference velocity $\bar{u}_{0r}$, the corresponding steady response of Equation (26) will be constant too, and its components can be computed for $i \in \{1, \dots, N\}$ upon the following equations (see e.g. Michałek, 2013):

$$\bar{\beta}_{ir} = \begin{cases} 0 & \text{if } \bar{\omega}_{0r} \equiv 0 \\ \text{Atan2}(\bar{a}_{ir}, \bar{b}_{ir}) & \text{if } \bar{\omega}_{0r} \not\equiv 0 \end{cases},$$

where $\bar{a}_{ir} = \bar{L}_i\bar{R}_{i-1r} + \bar{L}_{hi}\bar{R}_{ir}$, $\bar{b}_{ir} = \bar{R}_{ir}\bar{R}_{i-1r} - \bar{L}_i\bar{L}_{hi}$,

$$\bar{R}_{0r} = \bar{v}_{0r}/\bar{\omega}_{0r},$$

$$\bar{R}_{ir} = \text{sgn}(\bar{v}_{0r}/\bar{\omega}_{0r})\sqrt{\bar{R}_{i-1r}^2 - \bar{L}_i^2 + \bar{L}_{hi}^2},$$

while $\text{sgn}(z) = 1$ if $z \geq 0$, and $\text{sgn}(z) = -1$ if $z < 0$.

A2. Stability of zero-equilibrium for dynamics (38)

According to kinematics (3), one can write particular rows of dynamics (38) as follows:

$$\dot{\tilde{\beta}}_1 = \boldsymbol{c}^\top\boldsymbol{\Gamma}_1(\beta_{1r})\boldsymbol{u}_{0r} - \boldsymbol{c}^\top\boldsymbol{\Gamma}_1(\beta_{1r} - \tilde{\beta}_1)\boldsymbol{u}_{0r}, \qquad (A1)$$

$$\dot{\tilde{\beta}}_i = \boldsymbol{c}^\top\boldsymbol{\Gamma}_i(\beta_{ir})\prod_{j=i-1}^1 \boldsymbol{J}_j(\beta_{jr})\boldsymbol{u}_{0r}$$

$$- \boldsymbol{c}^\top\boldsymbol{\Gamma}_i(\beta_{ir} - \tilde{\beta}_i)\prod_{j=i-1}^1 \boldsymbol{J}_j(\beta_{jr} - \tilde{\beta}_j)\boldsymbol{u}_{0r} \qquad (A2)$$

for $i = 2, \ldots, N$. It is evident that $\tilde{\boldsymbol{\beta}} = \boldsymbol{0}$ is an equilibrium point of dynamics (38). One can check (by direct computations) that the following equality holds true: $\boldsymbol{J}_i(\beta_{ir} - \tilde{\beta}_i) = \boldsymbol{J}_i(\beta_{ir})\boldsymbol{R}_{hi}(\tilde{\beta}_i)$ for any $i = 1, \ldots, N$, where

$$\boldsymbol{R}_{hi}(\tilde{\beta}_i) = \begin{bmatrix} c\tilde{\beta}_i & (1/L_{hi})s\tilde{\beta}_i \\ -L_{hi}s\tilde{\beta}_i & c\tilde{\beta}_i \end{bmatrix}.$$

Thus, we can rewrite Equations (A1) and (A2) in the form which emphasises the lower-triangular structure of dynamics (38), that is,

$$\dot{\tilde{\beta}}_1 = f_1(\tilde{\beta}_1, t), \qquad (A3)$$

$$\dot{\tilde{\beta}}_i = f_i(\tilde{\beta}_1, \ldots, \tilde{\beta}_i, t), \quad i = 2, \ldots, N \qquad (A4)$$

where

$$f_1 = \boldsymbol{c}^\top[\boldsymbol{I} - \boldsymbol{J}_1(\beta_{1r})]\boldsymbol{u}_{0r} - \boldsymbol{c}^\top[\boldsymbol{I} - \boldsymbol{J}_1(\beta_{1r})\boldsymbol{R}_{h1}(\tilde{\beta}_1)]\boldsymbol{u}_{0r},$$

$$f_i = \boldsymbol{c}^\top[\boldsymbol{I} - \boldsymbol{J}_i(\beta_{ir})]\prod_{j=i-1}^1 \boldsymbol{J}_j(\beta_{jr})\boldsymbol{u}_{0r}$$

$$- \boldsymbol{c}^\top[\boldsymbol{I} - \boldsymbol{J}_i(\beta_{ir})\boldsymbol{R}_{hi}(\tilde{\beta}_i)\prod_{j=i-1}^1 \boldsymbol{J}_j(\beta_{jr})\boldsymbol{R}_{hj}(\tilde{\beta}_j)\boldsymbol{u}_{0r}.$$

Taylor linearisation of dynamics (A3) and (A4) at the equilibrium $\tilde{\boldsymbol{\beta}} = \boldsymbol{0}$ gives the following linear approximation:

$$\dot{\tilde{\boldsymbol{\beta}}} = \boldsymbol{A}(t)\tilde{\boldsymbol{\beta}}, \qquad (A5)$$

where $\boldsymbol{A}(t)$ is the lower-triangular matrix with all the non-zero off-diagonal elements (for $i = 2, \ldots, N, l = 1, \ldots, i - 1$)

$$a_{il}(t) = \boldsymbol{c}^\top[\boldsymbol{I} - \boldsymbol{J}_i^{-1}(\beta_{ir}(t))]\prod_{j=i}^l \boldsymbol{J}_j(\beta_{jr}(t))$$

$$\times \begin{bmatrix} 0 & (1/L_{hl}) \\ -L_{hl} & 0 \end{bmatrix}\prod_{j=l+1}^1 \boldsymbol{J}_j(\beta_{jr}(t))\boldsymbol{u}_{0r}(t)$$

uniformly bounded in t, and with eigenvalues equal to the diagonal elements of the form (for $i = 1, \ldots, N$)

$$a_{ii}(t) = -\left[\frac{L_{hi}}{L_i}s\beta_{ir}(t)\frac{1}{L_i}c\beta_{ir}(t)\right]\prod_{j=i-1}^1 \boldsymbol{J}_j(\beta_{jr}(t))\boldsymbol{u}_{0r}(t)$$

$$\overset{(5)}{=} -\frac{1}{L_i}[L_{hi}s\beta_{ir}(t)\ c\beta_{ir}(t)]\boldsymbol{u}_{i-1r}(t)$$

$$= -v_{ir}(t)/L_i < 0, \qquad (A6)$$

where $L_i > 0$ by construction, and the reference longitudinal velocities $v_{ir}(t) > 0$ for all $t \geq 0$ from assumption (see (r1) and condition (14)).

To assess stability of dynamics (A5), we have to separately consider two cases: when $\bar{\boldsymbol{u}}_{Nr} = \text{const}$ (corresponding to (s1)), and when $\bar{\boldsymbol{u}}_{Nr}(t)$ is time-varying (corresponding to (s2)). It is well known that in the case (s1) the reference joint-angles $\bar{\boldsymbol{\beta}}_r = \text{const}$ imply $\bar{\boldsymbol{u}}_{0r} = \text{inv}\boldsymbol{V}_0(\bar{\boldsymbol{u}}_{Nr}, \bar{\boldsymbol{\beta}}_r) \equiv \boldsymbol{u}_{0r} = \text{const}$. Constant tractor velocity $\boldsymbol{u}_{0r}$ corresponds to $\boldsymbol{\beta}_r = \text{const}$, and $\boldsymbol{u}_{ir} = [\omega_{ir}\ v_{ir}]^\top = \boldsymbol{V}^i(\boldsymbol{u}_{0r}, \boldsymbol{\beta}_r) = \text{const}$ for any $i = 1, \ldots, N$. Thus, in case (s1), matrix $\boldsymbol{A}(t) = \boldsymbol{A}$ becomes time-invariant, and the local uniform exponential stability of $\tilde{\boldsymbol{\beta}} = \boldsymbol{0}$ results directly from Equation (A6). In case (s2), one has to further investigate properties of matrix $\boldsymbol{A}(t)$ and its time-derivative $\dot{\boldsymbol{A}}(t)$. Since all the components of matrix $\boldsymbol{A}(t)$ are uniformly bounded, one can claim $\|\boldsymbol{A}(t)\| < \bar{A} < \infty$ for all $t \geq 0$. Next, one can write

$$\dot{a}_{ij}(t) = \boldsymbol{a}_{\beta ij}^\top\dot{\boldsymbol{\beta}}_r + \boldsymbol{a}_{uij}^\top\dot{\boldsymbol{u}}_{0r}, \quad i, j \in \{1, \ldots, N\}, \qquad (A7)$$

where $\boldsymbol{a}_{\beta ij}^\top \triangleq \partial a_{ij}/\partial\boldsymbol{\beta}_r$ and $\boldsymbol{a}_{uij}^\top \triangleq \partial a_{ij}/\partial\boldsymbol{u}_{0r}$. According to the forms of components $a_{ij}(t)$, by recalling Assumption A1, and due to the assumed boundedness of reference velocity $\boldsymbol{u}_{Nr}$ (see (r2)) one may conclude

$$\left\|\boldsymbol{a}_{\beta ij}^\top\right\| \leq \delta_{\beta ij}, \quad \left\|\boldsymbol{a}_{uij}^\top\right\| \leq \delta_{uij}, \qquad (A8)$$

where $\delta_{\beta ij} > 0$ and $\delta_{uij} > 0$ are some finite constants. Next, by recalling the forms of Equation (13) and matrix $\boldsymbol{S}_\beta$ in Equation (3), one may (conservatively) assess

$$\|\dot{\boldsymbol{\beta}}_r\| \leq \|\boldsymbol{S}_\beta(\boldsymbol{\beta}_r)\prod_{j=1}^N \boldsymbol{J}_j^{-1}(\beta_{jr})\|\ \|\boldsymbol{u}_{Nr}\| \leq \delta_s\|\boldsymbol{u}_{Nr}\|,$$

and, by analogy to the above,

$$\|\dot{\bar{\boldsymbol{\beta}}}_r\| \leq \bar{\delta}_s\|\bar{\boldsymbol{u}}_{Nr}\|,$$

where $0 < \delta_s, \bar{\delta}_s < \infty$ under Assumptions A1–A2. Furthermore, since $\boldsymbol{u}_{0r} \equiv \bar{\boldsymbol{u}}_{0r} = \prod_{j=1}^N \bar{\boldsymbol{J}}_j^{-1}(\bar{\beta}_{jr})\bar{\boldsymbol{u}}_{Nr} =: \bar{\boldsymbol{P}}(\bar{\boldsymbol{\beta}}_r)\bar{\boldsymbol{u}}_{Nr} = [\bar{\boldsymbol{p}}_1(\bar{\boldsymbol{\beta}}_r)\ \bar{\boldsymbol{p}}_2(\bar{\boldsymbol{\beta}}_r)]\bar{\boldsymbol{u}}_{Nr}$, and since the components of matrix $\bar{\boldsymbol{P}}(\bar{\boldsymbol{\beta}}_r)$ are bounded (under A1 and A2) combinations of products of

trigonometric functions, we can assess

$$
\begin{aligned}
\|\dot{\boldsymbol{u}}_{0r}\| &= \left\| \dot{\bar{\boldsymbol{P}}}(\bar{\boldsymbol{\beta}}_r)\bar{\boldsymbol{u}}_{Nr} + \bar{\boldsymbol{P}}(\bar{\boldsymbol{\beta}}_r)\dot{\bar{\boldsymbol{u}}}_{Nr} \right\| \\
&\leq \left\| \left[\frac{\partial \bar{\boldsymbol{p}}_1}{\partial \bar{\boldsymbol{\beta}}_r} \dot{\bar{\boldsymbol{\beta}}}_r \; \frac{\partial \bar{\boldsymbol{p}}_2}{\partial \bar{\boldsymbol{\beta}}_r} \dot{\bar{\boldsymbol{\beta}}}_r \right] \right\| \|\bar{\boldsymbol{u}}_{Nr}\| + \left\| \bar{\boldsymbol{P}}(\bar{\boldsymbol{\beta}}_r) \right\| \left\| \dot{\bar{\boldsymbol{u}}}_{Nr} \right\| \\
&\leq \chi \left\| \frac{\partial \bar{\boldsymbol{p}}_j}{\partial \bar{\boldsymbol{\beta}}_r} \right\| \|\dot{\bar{\boldsymbol{\beta}}}_r\| \|\bar{\boldsymbol{u}}_{Nr}\| + \left\| \bar{\boldsymbol{P}}(\bar{\boldsymbol{\beta}}_r) \right\| \left\| \dot{\bar{\boldsymbol{u}}}_{Nr} \right\| \\
&\leq \chi \rho_1 \bar{\delta}_s \|\bar{\boldsymbol{u}}_{Nr}\|^2 + \rho_2 \left\| \dot{\bar{\boldsymbol{u}}}_{Nr} \right\| \leq (\chi \rho_1 \bar{\delta}_s \bar{\delta}_1^2 + \rho_2 \bar{\delta}_2)
\end{aligned}
$$

for some $j \in \{1, 2\}$ and some finite constants $\chi > 0$ and $\rho_1, \rho_2 > 0$, where we have used the fact about equivalence of matrix and vector norms and the inequalities taken from condition (s2). Now, by using the inequality derived above

together with inequalities (A8), one can claim that (see Equation (A7)) $\forall t \geq 0 \; |\dot{a}_{ij}(t)| \leq \delta_{\beta ij} \delta_s \delta_1 + \delta_{uij} (\chi \rho_1 \bar{\delta}_s \bar{\delta}_1^2 + \rho_2 \bar{\delta}_2)$, and consequently (for a spectral norm of $\dot{\boldsymbol{A}}$):

$$
\begin{aligned}
\|\dot{\boldsymbol{A}}(t)\| &\leq N \max_{i,j} |\dot{a}_{ij}(t)| \\
&\leq N \left[\delta_{\beta ij}^* \delta_s \delta_1 + \delta_{uij}^* (\chi \rho_1 \bar{\delta}_s \bar{\delta}_1^2 + \rho_2 \bar{\delta}_2) \right] \\
&\stackrel{(30)}{=} N \left[\delta_{\beta ij}^* \delta_s \bar{\delta}_1 / \eta_1 + \delta_{uij}^* (\chi \rho_1 \bar{\delta}_s \bar{\delta}_1^2 + \rho_2 \bar{\delta}_2) \right] \quad \text{(A9)}
\end{aligned}
$$

for all $t \geq 0$, where $\delta_{\beta ij}^* = \max_{i,j}(\delta_{\beta ij})$ and $\delta_{uij}^* = \max_{i,j}(\delta_{uij})$. By ensuring that $\bar{\delta}_1$ and $\bar{\delta}_2$ are sufficiently small (postulated in (s2)), the right-hand side of Equation (A9) can be made small enough to satisfy the sufficient condition for asymptotic stability of linear time varying (LTV) system (A5); see Zhu (1993).